Portland State University

PDXScholar

1-1-1983

A mechanistic study of the electrochemical formation of CdS CdSe semiconducting films

Mario Aparicio-Razo
Portland State University

Follow this and additional works at: https://pdxscholar.library.pdx.edu/open_access_etds

Let us know how access to this document benefits you.

A MECHANISTIC STUDY OF THE ELECTROCHEMICAL

FORMATION OF CdS/CdSe SEMICONDUCTING FILMS

by

MARIO APARICIO-RAZO

A dissertation submitted in partial fulfillment of the
requirements for the degree

DOCTOR OF PHILOSOPHY
in
ENVIRONMENTAL SCIENCES AND RESOURCES: CHEMISTRY

Portland State University

TO THE OFFICE OF GRADUATE STUDIES AND RESEARCH:

The members of the Committee approve the dissertation of Mario Aparicio-Razo presented May 13, 1983.

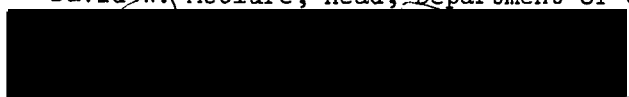David K. Roe, Chairman

Jonathan J. Abramson

Nicholas G. Eror

Carol R. Gatz

John G. Rueter

APPROVED:

David W. McClure, Head, Department of Chemistry.

Robert O. Tinnin, Director, Environmental Sciences and Resources.

William W. Paudler, Dean, College of Liberal Arts and Sciences.
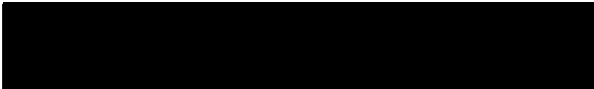
Stanley E. Rauch, Dean of Graduate Studies and Research.

AN ABSTRACT OF THE DISSERTATION OF Mario Aparicio-Razo for the

Doctor of Philosophy in Environmental Sciences and Resources: Chemistry

presented May 13, 1983.
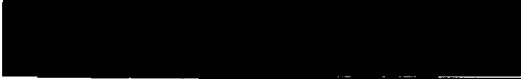
Title: A Mechanistic Study of the Electrochemical Formation of

      CdS/CdSe Semiconducting Films

APPROVED BY MEMBERS OF THE DISSERTATION COMMITTEE:

David K. Roe, Chairman

Jonathan J. Abramson

Nicholas G. Eror

Carol R. Gatz

John G. Rueter

Cadmium sulfide and cadmium selenide are important materials for
applications such as photoconductive cells, photovoltaic cells and other
electrooptical devices. Generally, these devices use single crystals.
However, reasonable efficiencies have been observed by using polycrystal-
line films on conducting substrates, which are easier to make and pro-

vide considerable savings on materials and energy.

Polycrystalline CdS/CdSe films have been made by sputtering and solution spraying, compound evaporation, chemical vapor deposition, and many others. A recent technique involves the electrochemical deposition of CdS and CdSe from nonaqueous solvents. Preparation of these films is based upon the cathodic deposition from a nonaqueous solution of a cadmium salt and elemental sulfur and/or selenium. Although the technique is simple, no mechanistic information is known to optimize the conditions in which films of controlled stoichiometry, doping and crystallinity are made.

This research has the purpose to understand the mechanism of the formation of polycrystalline films of CdS and CdSe by electrochemical deposition in dimethylsulfoxide. This approach to the problem makes use of electrochemical techniques such as rotating ring disc electrode, linear scan voltammetry, high pressure liquid chromatography coupled with ultraviolet and electrochemical detection.

By the rotating ring disc electrode technique, we have studied the kinetic parameters for the reduction of sulfur, selenium, cadmium, and the electrochemical formation of CdS and CdSe for temperatures from 25 - $100^{\circ}C$. The results show that rates of initial electron transfer for the reduction of these species are moderately rapid, and secondly, that the reverse reaction is irreversible and involves additional steps. Studies of solubility of selenium with temperature reveal that its solubility is enhanced by the addition of sulfur. Understanding the electrochemical behavior of sulfur-selenium mixtures is of great importance to produce mixed semiconductive films with more adequate bandgaps for use with so-

lar spectrum. Electrochemistry of sulfur-selenium mixtures are no different from that of sulfur alone. High pressure liquid chromatography separations with spectroscopic and electrochemical detectors have shown that sulfur solutions contain S_6 and S_7 fractions which are not electrochemically active.

ACKNOWLEDGEMENTS

TABLE OF CONTENTS

LIST OF TABLES

LIST OF FIGURES

CHAPTER I

INTRODUCTION

Cadmium sulfide and cadmium selenide are important materials for applications such as photoconductive cells, photovoltaic cells, photo-electrochemical cells, and other electrooptical devices (1-6). Generally, these devices use single crystals. However, reasonable efficiencies have been observed by using polycrystalline films on conducting substrates.

Thus far, these films have been formed by vapor deposition techniques (7-9), heterogeneous precipitation from solution (10-14), flash evaporation (15), press sintered (16-17), aqueous and paste painting (18-20), electrochemical codeposition (21-22), anodization of a metal in sulfur or selenium solutions (23), cathodically deposited from aqueous solutions (24-28), and even electrophoretically (29). Heat treatment followed almost all of the methods used.

The purpose of this research is to try to understand the mechanism of formation of CdS and CdSe by electrochemical deposition from nonaqueous solvents, in particular with dimethylsulfoxide (DMSO) as the solvent. Preparation of these films is based upon cathodic deposition from a nonaqueous solution of a cadmium salt and elemental sulfur and/or selenium. The solution may contain an inert electrolyte, such as sodium tetrafluoroborate (TFB) to improve electrolytic conduction.

Cathodic electrodeposition of metal chalcogenides has been the object of the work of two different groups (30, 31). They have reported deposits that produce photopotentials in aqueous sulfur sulfide solutions, and that doping agents could be incorporated in the films during the electrochemical process.

Baranski and Fawcett (31-33) reported films of CdS, CdSe, CdS-CdSe, PbS, Cu_2S, and many others electrodeposited on Pt, Au, stainless steel, Ni, Zn, and glass covered with SnO_2 from elemental chalcogenide, and the metal salt solutions from solvents such as DMSO, DMF and ethyl glycol. The overall reaction reported is
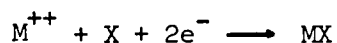
$$M^{++} + X + 2e^- \longrightarrow MX$$ 1

They propose a mechanism in which freshly electrodeposited metal monolayer reacts with the dissolved chalcogenide. X-ray diffractometer patterns compare favorably with those for β-CdS. A Rutherford spectrum for α-particles back-scattered from the CdS deposits gave two peaks, one for Cd and one for S. From these peaks the film composition was estimated to be uniform in depth with a sulfur to cadmium ratio of $0.9^+_- 0.1$ to one. For the CdS Se films, three peaks were observed and the sulfur peak decreased as the selenium concentration was increased. However, an 81% coulombic efficiency was observed, the remaining charge was attributed to secondary reactions involving oxygen and/or water, or to the reduction of sulfur contained in sulfur-oxygen species.

Roe, Li, and Gerischer (30) have also reported the cathodic deposition of metal sulfides and selenides. The proposed reaction sequence was reported to be

$$M^{n+} + ne^- = M_{(surf)} \qquad\qquad 2a$$

$$X_m + qM_{(surf)} = M_q X_{p(surf)} + X_{(m-p)} \qquad\qquad 2b$$

or

$$X_m + 2e^- = X_m^{2-} \qquad\qquad 3a$$

$$X_m^{2-} + qM^{n+} = M_q X_{p(surf)} + X_{(m-p)} \qquad\qquad 3b$$
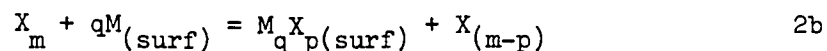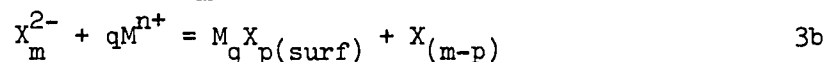
Where X_m and $X_{(m-p)}$ represent a sulfur or selenium species of un-specified molecularity.

A voltammetric study of the electrodesposition precess of CdS showed that initially, underpotential deposits of cadmium reacted with S_8 or absorbed sulfur on the electrode surface at room temperature. At 95°, the reaction is more complex, and direct reduction of S_8 to polysulfides competed with the electrodeposition of CdS.

Hogle (34) has investigated the non-faradic reaction of Cd and S in DMSO by UV-visible and atomic absorption spectroscopy. From his results he concluded that reaction 2b yielded a soluble product having a ratio of S/Cd greater than one. Cd^{+2} has shown to have a capacity to react with polysulfides, and therefore, a side-reaction competes with the formation of CdS by reaction 2b. Cadmium metal has been shown to react with S_8 to form CdS_p and soluble polysulfide complexes. CdS_p complexes have greater solubility than CdS in DMSO, and tend to stay in solution.

The purpose of this research is to obtain kinetic information about the reduction of cadmium ions, sulfur, and selenium in DMSO and their soluble products. This information in turn will be used to understand the mechanism of the reaction of formation of CdS and CdSe

in DMSO. To achieve our goal, electrochemical measurements by linear scan voltammetry, rotating ring disc electrode and high pressure liquid chromatography coupled with ultraviolet and electrochemical detectors. Experimental variables include solution temperature, concentration of reactants and electrochemical conditions.

A particularly significant experimental detail is the use of a rotating ring disc electrodes (RRDE) in this study. However, there are no RRDE commercially available which are usable at elevated temperatures. This problem was solved by developing a prototype ceramic based ring disc electrode which could be used at elevated temperatures.

The rotating ring disc electrode is almost unique for this study. The ring electrode is used to detect instantaneously soluble species produced at the disc electrode. With a RRDE, steady state is attained quickly and measurements can be made with great precision. In addition, at steady state conditions, double layer charging does not enter into measurements and the rates of mass transfer at the electrode are reproducible and known. Since the rates of mass transfer are much larger than the rates of diffusion, the relative contribution of the effect of mass transfer rates to the electron transfer kinetics can be small.

Electrochemistry of many common ions in nonaqueous solvents has appeared in the literature and has been summarized by Mann and Barnes (35). The majority of the reactions have been studied by dropping mercury electrode, and the reactions are generally diffusion controlled. In our work deposits of cadmium are achieved

by RRDE and the kinetics of the electron transfer studied.

Studies of sulfur reduction (36) in DMSO reveal that poly-sulfides are formed, which is also the case in aqueous solutions (37). Spectrometric measurements by Giggenbach has shown that chain length is temperature dependant. Recent work by Streudel and Tebbe (38, 39) using HPLC has shown that S_6, S_7 and S_8 are the major species of

sulfur in CS_2 solutions. Our work has shown that it is also the case in DMSO. Furthermore, S_8 was reduced for the potential range studied. S_6 and S_7 are more likely absorbed on the electrode surface. RRDE studies have shown that this reduction is kinetically controlled for temperatures up to $100^{\circ}C$.

Nothing is know for selenium in DMSO. Our studies followed a parallel approach to that of sulfur. We found the solubility of selenium in DMSO was increased by the addition of sulfur. Electro-chemical studies by RRDE were conducted for temperatures up to $100^{\circ}C$. The understanding of the electrochemical properties of S_xSe_y are significant for the possible formation of CdS-CdSe semiconductors.

CHAPTER II

EXPERIMENTAL

Reagents

Analytical reagent grade chemicals were used unless otherwise
stated. All aqueous solutions were prepared from quartz distilled wa-
ter and were stored in glass flasks. Working solutions were prepared
by addition of an aliquot of the stock solution by pipet or buret and/or
a weighed amount of the required reagent, followed by dilution to vo-
lume by the required solvent.

Cadmium chloride. Cadmium chloride ($CdCl_2 \cdot 2\frac{1}{2}H_2O$) was ground to a
fine powder with mortar and pestle and dried overnight at $110^\circ C$.

Cadmium nitrate. Cadmium nitrate was used without further purifi-
cation.

Dimethylsulfoxide. Dimethylsulfoxide (DMSO) technical grade from
the Crown Zellerbach Company, and analytical reagent grade from the T.
Baker Chemical Company were used without further purification. UV-visi-
ble spectra from both sources were found to be optically pure from 260
to 750 nm. Water content was determined by the Karl Fischer titration
was found to be 0.005% by weight.

Gold (III) chloride. Gold(III) chloride plating solutions were
prepared by dissolving 0.3 g gold metal in 10 mL of 1:1 HNO_3:HCl. The
acid was evaporated to almost dryness, 10 mL of 6F HCl were added and
evaporated, and then diluted to 10 mL with quartz distilled water.

Karl Fischer Reagent. Karl Fischer reagent and reagent diluent from the T. Baker Chemical Company were used without further purification.

Methanol. HPLC grade methanol was used without further purification.

Nitric acid. Nitric acid was used without further purification.

Potassium chloride. Potassium chloride was used without further purification.

Potassium ferricyanide. Potassium ferricyanide was used without further purification.

Selenium. Pure selenium (99.999%) was used without further purification.

Sodium borohydride. Reagent grade sodium borohydride was used without further purification.

Sodium tetrafluoroborate. Reagent grade sodium tetrafluoroborate was recrystallized from quartz distilled water.

Sulfur. Pure sulfur (99.999%) was used without further purification.

Tetraethylammonium perchlorate. Polarografic grade tetraethylammonium perchlorate (TEAP) was used without further purification.

Water. Triply quartz distilled water was used and stored in polypropylene bottles.

Equipment

High pressure liquid chromatograph. Water Associates liquid chromatograph, Model 6000A was used, equipped with a Model 440, 254 nm wavelength absorbance detector, a Spectra Physics SP 8440 variable wavelength detector, a 20 μL Rheodine syringe loading sample injector Model 7125 and a Beckman Ultrasphere ODS 5 μC$_{18}$ reversed phased column.

Electrochemical flow cell. A LC17 Bioanalyical Systems electrochemical thin layer flow cell, equipped with a gold working electrode and a glassy carbon counter electrode, was connected to the outlet of the absorbance detector, in the typical three electrode arrangement to a potentiostat with current integration.

Ultraviolet-visible. A Beckman Model 26 spectrophotometer with 1 cm quartz cuvettes was used for UV-visible spectra.

Potentiostat and rotating electrode speed control. A dual potentiostat and rotating electrode speed control was built in this laboratory. Prototype potentiostat equipped with current integrator was built by the Fritz Haber Institute in Berlin, Germany.

Rotating ring-disc electrode. A teflon insulated rotating gold ring-disc electrode (RRDE) Model TB16 from Pine Instruments Company (r_1= 0.382 cm, r_2= 0.399 cm, r_3= 0.422 cm), and a prototype (r_1= 0.338 cm, r_2= 0.400 cm, r_3= 0.600 cm) ceramic insulated, gold RRDE for high temperatures measurements were used, as shown in Figure 1.

Gold microelectrode. A gold plated platinum electrode, 1 mm in diameter, sealed in glass, made in this laboratory was used.

Reference and counter electrode. An aqueous Ag/AgCl reference electrode and a 4 cm^2 platinum foil was used as a counter electrode.
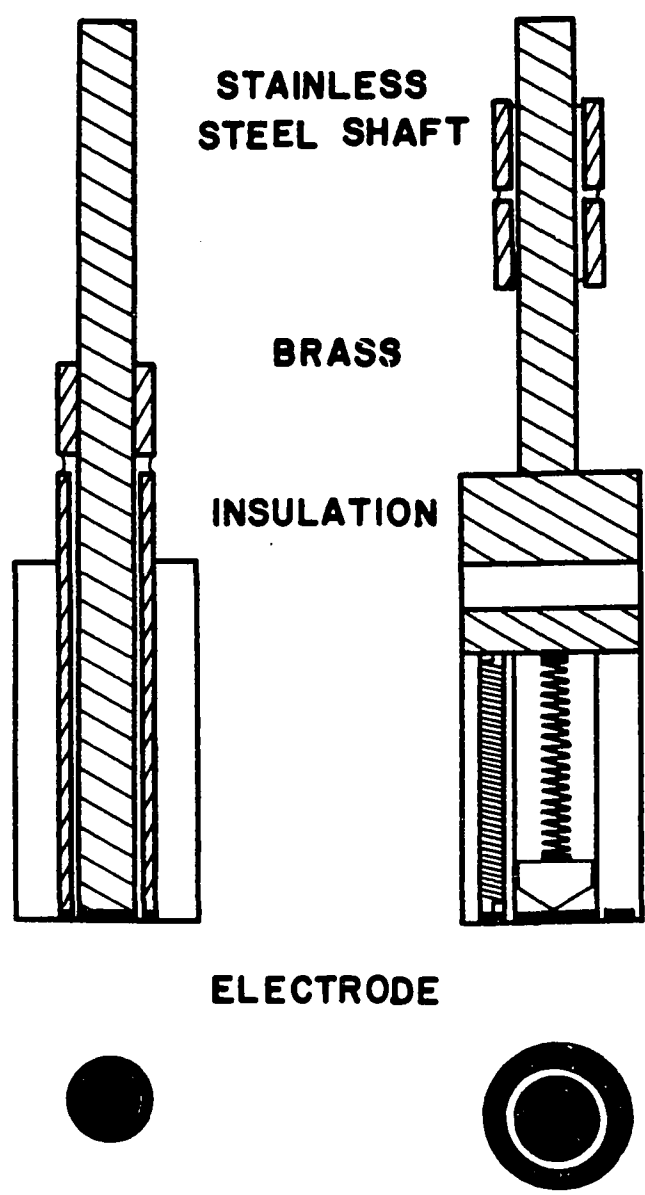
Figure 1. Rotating Ring-Disc Electrode

<u>Cell</u>. Glass cells of 40 and 100 mL, with connections for reference and counter electrodes, as well as for gas purge, were used for all measurements (See Figure 2).

<u>Calculations</u>. All calculations were carried out on a Hewlett Packard pocket calculator HP-25C and on a Honeywell 66/20 computer system. All data were analyzed by linear regression using the program LSQL written in Fortran by B. W. Brown. Where required, standard statistical methods were applied to the data. In such cases, the results are reported as the mean value plus and minus the standard deviation.

Experimental methods and procedures

<u>Determination of the solubility of selenium in DMSO</u>. The solubility of selenium in DMSO was determined as a function of temperature for the range of 23 to 140°C. Excess selenium powder was added to 100 mL of DMSO, purged with nitrogen, heated to the desired temperature, and equilibrated for three to eight hours. Aliquots of 10 to 20 mL of the selenium solution were drawn, the solvent evaporated, and the selenium weighed in constant weight crucibles. Aliquots of the solvent alone were also taken as a control.

The solubility of selenium in DMSO in the presence of sulfur was determined in the same way. Sulfur was added at a known concentration below saturation. The weight of sulfur in every sample was then subtracted from the dry selenium-sulfur weights.

UV spectra of the selenium, sulfur, and selenium-sulfur solutions were recorded from 240 to 360 nm using DMSO as a reference.

Solubility of selenium in DMSO in the presence of toluene and ace-
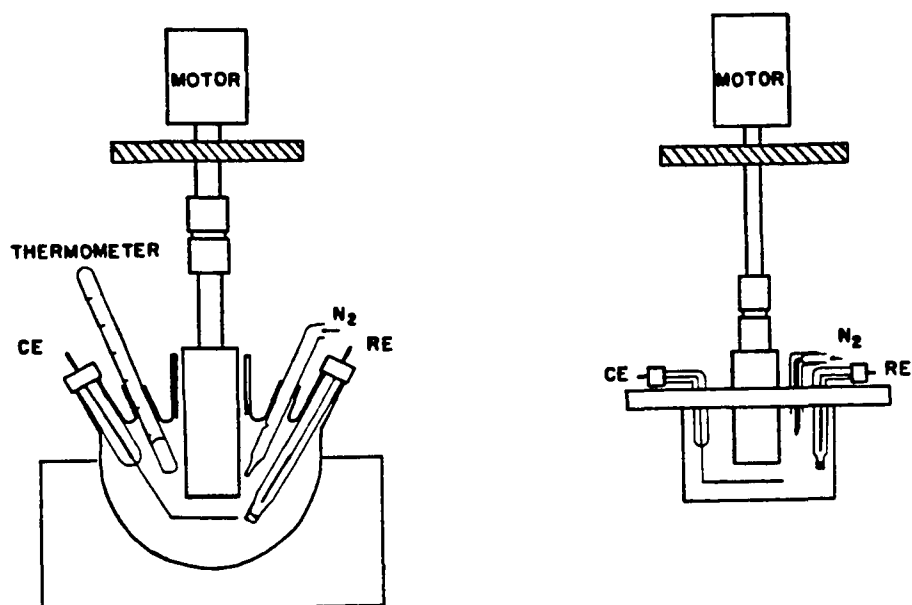
Figure 2. Electrochemical Cells for RRDE Studies.

tonitrile, as well as selenium in sulfolane were also determined fol-
lowing the same method.

HPLC analysis. Samples of 20 μL of sulfur and/or selenium solu-
tions in DMSO or methanol were injected in the HPLC and eluted with
methanol at 1.6 mL/min ($\sim$2500 psi), followed by UV detection over the
range of 250 - 300 nm and by an electrochemical flow cell over the po-
tential range of -0.35 to -1.60 V versus Ag/AgCl.

Reaction of cadmium with sulfur and/or selenium. Freshly preci-
pitated cadmium was reacted with sulfur and/or selenium in DMSO. Pre-
cipitated cadmium samples were prepared by the reduction of aqueous cad-
mium ion, of 1 M $Cd(NO_3)_2$, with three times the stoichiometric amount
of crystalline sodium borohydride according to the reactions

$$Cd^{+2} + 2BH_4^- = Cd + H_2 + B_2H_6 \qquad\qquad 4$$

$$B_2H_6 + 6H_2O = 2H_3BO_3 + 6H_2 \qquad\qquad 5$$
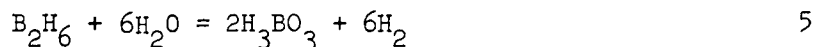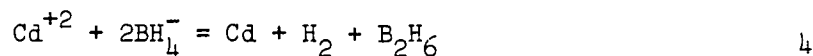
Cadmium samples were collected in a glass fritted funnel, washed
with distilled water, and finally washed with three 10 mL aliquots of
DMSO. The last aliquot of DMSO was kept for a control.

Aliquots of 10 mL of sulfur and/or selenium solution were passed
through the glass fritted funnel containing the freshly precipitated
cadmium. The sulfur and/or selenium solutions were analyzed before and
after the reaction by HPLC.

Supporting electrolytes. Solutions of 0.1 F $NaBF_4$ were prepared
by dissolving the appropriate amounts of $NaBF_4$ in DMSO. All solutions
were purged with nitrogen and electrolyzed for one hour using a platinum
gauze as the working electrode at -1.2 V versus Ag/AgCl.
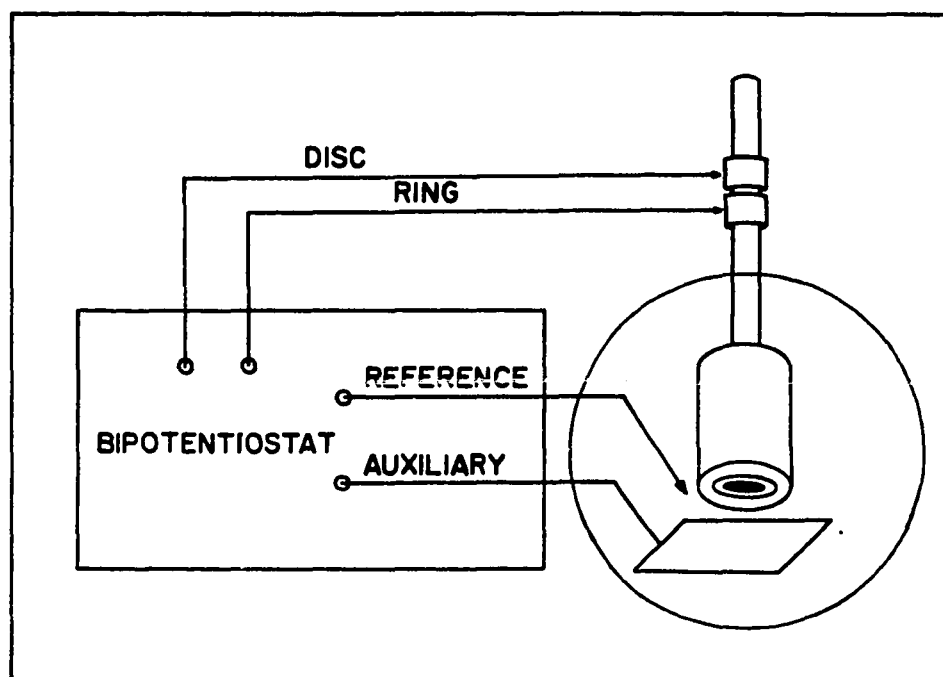
Figure 3. Dual Potentiostat for RRDE Measurements.

Electrode pretreatment. The microelectrode and the ceramic insu-
lated RRDE were electroplated with a Au(III) chloride wolution at 50°C
and current density of 1 mA/cm^2, for 2 - 20 minutes. The electrode was
rinsed with water and polished to a mirror finish with 0.3 μm alumina.
The electrode was rinsed with DMSO before introduction into the cell.
The microelectrode and RRDE's were preconditioned in the supporting elec-
tolyte by cyclic scanning for approximately 15 - 30 minutes and the re-
sidual current recorded at different scan rates, rotation rates, and
temperatures. All of the electrochemical measurements for the micro-
electrode, RRDE, and flow cell were made with a dual potentiostat, or
with an ordinary (three electrode) potentiostat equipped with current
integrator. A schematic diagram of the electrochemical system is shown
in Figure 3.

Rotating ring-disc electrode. The RRDE is constructed with a cen-
tral disc surrounded by a concentric insulating annulus, followed by a
concentric ring electrode as depicted in Figure 1. The electrode was
developed by Frumkin and Nekrasov (43, 44). Because of its construction,
potentials of the ring and disc can be controlled independently. Experi-
ments can be performed which use the ring electrode to provide addi-
tional information about processes occurring on the disc electrode. The
disc electrode can also be used as a source of species with the ring
electrode as a detector of unstable species.

The equation that relates the current at the disc electrode and the
rotation rate was first derived by Levich (45) in 1942. The equation
predicts that the limiting current should be proportional to the square
root of the rotation rate as described by equation 6

$$i_{D_{lim}} = 1.554 \ nAFD^{2/3} \ \nu^{-1/6} \ w^{1/2} \ C^* \qquad\qquad 6$$

where n is the number of electrons, A the area of the electrode in cm^2, ν is the kinematic viscosity in $cm^2 s^{-1}$, D is the diffusion coefficient in $cm^2 s^{-1}$, F is the faraday constant in Amp s mol^{-1}, w is in hertz, and C^* is the bulk concentration in mol cm^{-3}.

For the ring, the mass transfer is larger than that for the disc at a given rotation rate, because the flow of fresh solution to it occurs radially from the area inside the ring as well as normally from the bulk of the solution. The equation for the limiting ring current is described by equation 7 (46, 47).

$$i_{R_{lim}} = 1.554 \ nF\pi(r_3^3 - r_2^3)^{2/3} \ D^{2/3} \ \nu^{-1/6} \ w^{1/2} \ C^* \qquad 7$$

where r_2 and r_3 are the inner and outer radii of the ring electrode in cm.

The ring and disc currents are related by the collection efficiency (N_o). The collection efficiency is defined as the ratio of the ring current to the disc current at a given potential E, as shown in Figure 4.

$$N_o = - \frac{i_{R_{lim}}}{i_{D_{lim}}} \qquad\qquad 8$$
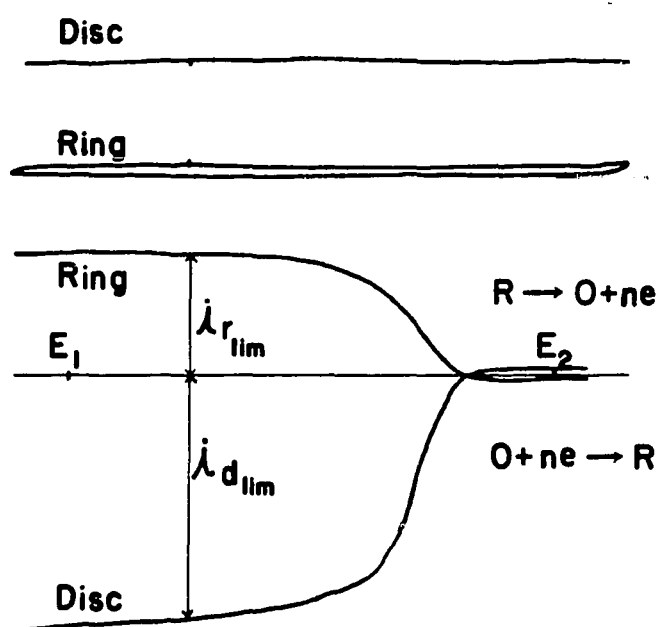
$$\frac{-\dot{\lambda}_r}{\dot{\lambda}_d} = N$$

Figure 4. Collection Efficiency.

The collection efficiency is a characteristic of each electrode and may be calculated from the geometry of the electrode since it depends only on r_1, r_2, and r_3. The collection effeciency can also be determined experimentally for an electrode by measuring the ratio $-i_{R_{lim}} / i_{D_{lim}}$ for a system

$$O + ne^- = R \qquad\qquad 9$$

where R is more stable. R is produced at the disc and is reoxidized at the ring. The collection efficiency is independent of the rotation rate.

Collection efficiency for the RRDE. The collection efficiency for the RRDE's was determined experimentally using $Fe(CN)_6^{-3}$ / $Fe(CN)_6^{-4}$ in 0.1 F H_2SO_4. The RRDE was rotated at 500. 1000. 2000, 3000, and 5000 rpm and scanned from +0.3 to -0.8 V versus Ag/AgCl at 20 mV/s. The ring and disc currents were measured at E_D = -0.5 V while the ring was kept at +0.1 V. The collection efficiency was determined to be 0.547 for the teflon electrode and 0.493 for the ceramic electrode. The results agreed within 1% of the theoretical values calculated from the equations given by Albery and Hitchman (46).

Reaction at the RRDE. The rotating disc electrode was scanned for potentials where reaction 9 occurs. Disc currents measurements were made at the plateau of the limiting currents for the different rotation rates, and corrected for the residual currents at the given potential. Intermediate products were searched for by scanning the ring at potentials (E_R) where reaction

$$R - ne^- = C \qquad\qquad 10$$

occurs, and where C may or may not be equal to 0, while the disc potential was set to produce R. From the ring scans, a ring potential (E_R) was selected to follow the reoxidation of the soluble product(s) for the different rotation rates.

Kinetic currents and diffusion coefficients. For reversible reactions i varies as $w^{\frac{1}{2}}$ at any potential. A deviation of a plot versus $w^{\frac{1}{2}}$ from a straight line that intersects the origin suggests some kinetic step involved in the electron transfer reaction. Should the reaction be completely irreversible a kinetic current (i_k) can be defined as

$$i_k = nFA\ k_f(E)C^{\bullet} \qquad\qquad 11$$

Therefore, the total observed current (i) at the disc for an irreversible reaction can be expressed as

$$\frac{1}{i} = \frac{1}{i_k} + \frac{1}{i_L} = \frac{1}{i_k} + \frac{1}{1.554\ nFAC\ D^{2/3}\sqrt{}^{-1/6}w^{\frac{1}{2}}} \qquad\qquad 12$$

It is clear from equation 12, that $i/w^{\frac{1}{2}}C$ is constant when i_k is very large. When this is not the case the plot of i versus $w^{\frac{1}{2}}$ will be bent toward the limit $i = i_k$ as $w^{\frac{1}{2}}$ goes to infinity. A plot of $1/i$ versus $1/w^{\frac{1}{2}}$ should be linear and can be extrapolated to $w^{-\frac{1}{2}} = 0$ to obtain i_k^{-1} (58).

From plots $(i/AC)^{-1}$ versus $w^{-\frac{1}{2}}$ the kinetic currents were determined and with equation 11 the heterogeneous rate constants for the forward reaction in the reduction of sulfur, selenium and cadmium ion were calculated. From the slopes of these graphs and equation 6, the diffusion coefficients were calculated.

CHAPTER III

RESULTS

Selenium

Solubility of selenium. The solubility of selenium in DMSO

follows an exponential growth with temperature for the range of 20°

to 140°C, as shown in Figure 5. The solubility can be expressed in

terms of the following expression, where the concentration of

selenium is expressed in mM (as Se).

$$\log \text{Se} = -1000.9 \frac{1}{T} + 2.93 \qquad\qquad 13$$

From the UV spectrum for selenium in DMSO the absorbance was

measured at 261 nm. The molar absorptivity $(\mathcal{E})$ was found to be

$(11.47 \pm 0.01) \times 10^2$ L mole^{-1}cm^{-1} by measuring a range of standards

$(4.3 \times 10^{-5}$ to 1.9×10^{-4} M). Beer's law was obeyed over the concen-

tration range studied. The additions of small amounts of sulfur

enhances the selenium solubility, for the range of temperatures

$50-100^\circ$C as shown in Figure 6. Addition of more than 0.25 mM of

sulfur does not continue to enhance selenium solubility. (See

Figure 6.) The UV spectra for sulfur-selenium solutions do not show

appreciable changes compared to the spectrum of selenium. For sulfur

concentrations larger than 0.25 mF, the UV spectrum for sulfur-

selenium starts to resemble the sulfur spectrum.
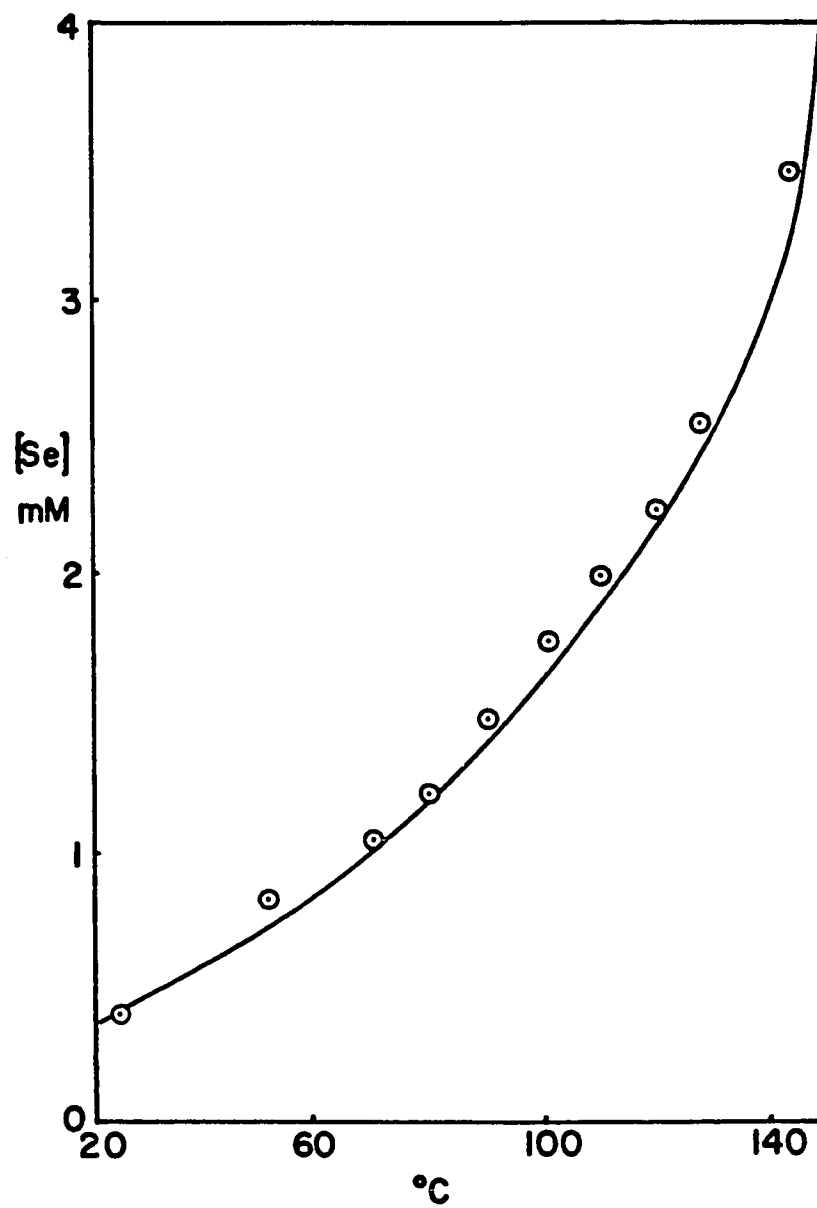
Figure 5. Solubility of Selenium as a Function of Temperature.
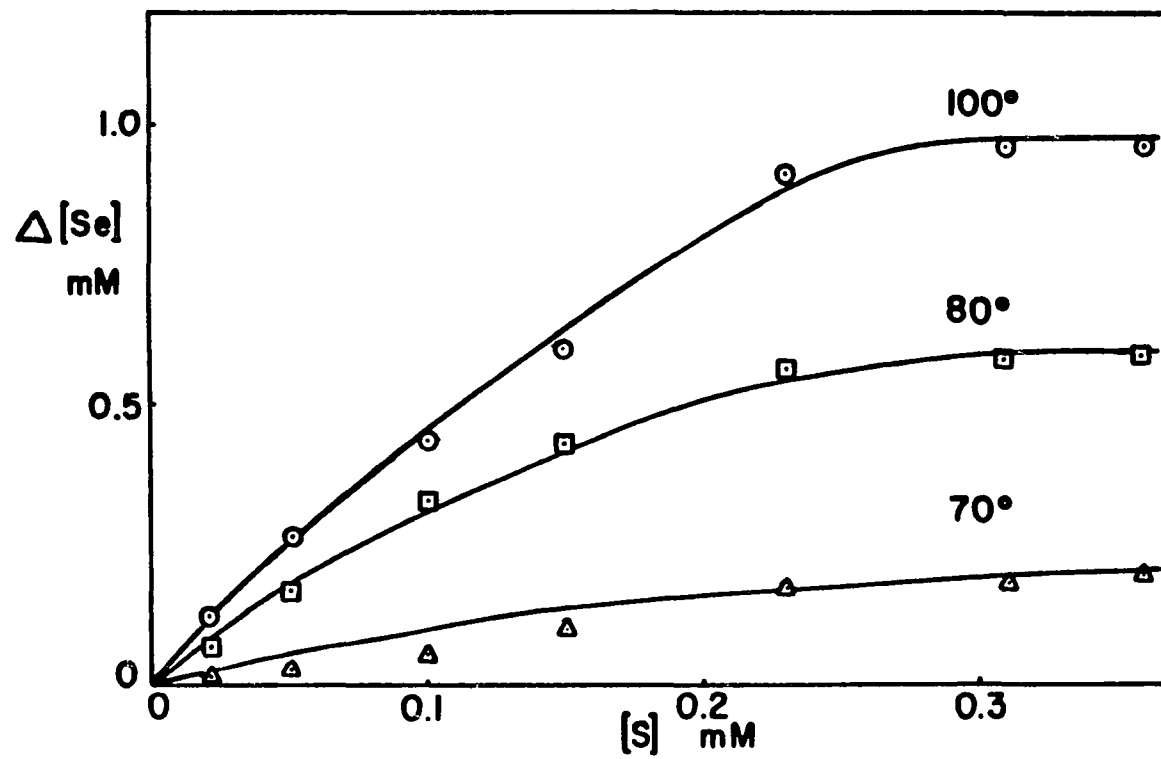
Figure 6. Increase of Selenium Solubility in DMSO in the Presence of Sulfur.

Electrochemistry of selenium. The electrochemistry of selenium was studied over the potential range of 0.4 to -1.6 v versus Ag/AgCl. The reduction of selenium starts at -1.2 V reaching a diffusion plateau at -1.4 V. A typical scan is shown in Figure 7.

The concentrations studied were under the saturation concentration at room temperature (Se_8 = 4.25 x 10^{-5}F). At concentrations greater than this value, a film of elemental selenium precipitates on the surface of the electrode, preventing further reduction.

The disc currents show some curvature on plots of i_L versus $w^{1/2}$, particularly for high values of $w^{1/2}$, as shown in Figure 8, for concentrations under 4.25 x 10^{-5} . The observed ring currents agreed with those predicted from the collection efficiency (N_o). The kinetic current was determined from the plots of $(i_L/AC)^{-1}$ versus $w^{-1/2}$, as shown in Figure 9.

The diffusion coefficient for selenium was calculated from the slopes of AC/i_L versus $w^{-1/2}$ and equation 1, using the values of the kinematic viscosity from viscosity and density data given by Janz and Tomkins (54). The average value of D was (5.51 $\pm$ 0.63) x 10^{-5} cm^2/s.

Table I presents the heterogeneous rate constant k^o for the reduction of selenium at room temperature.
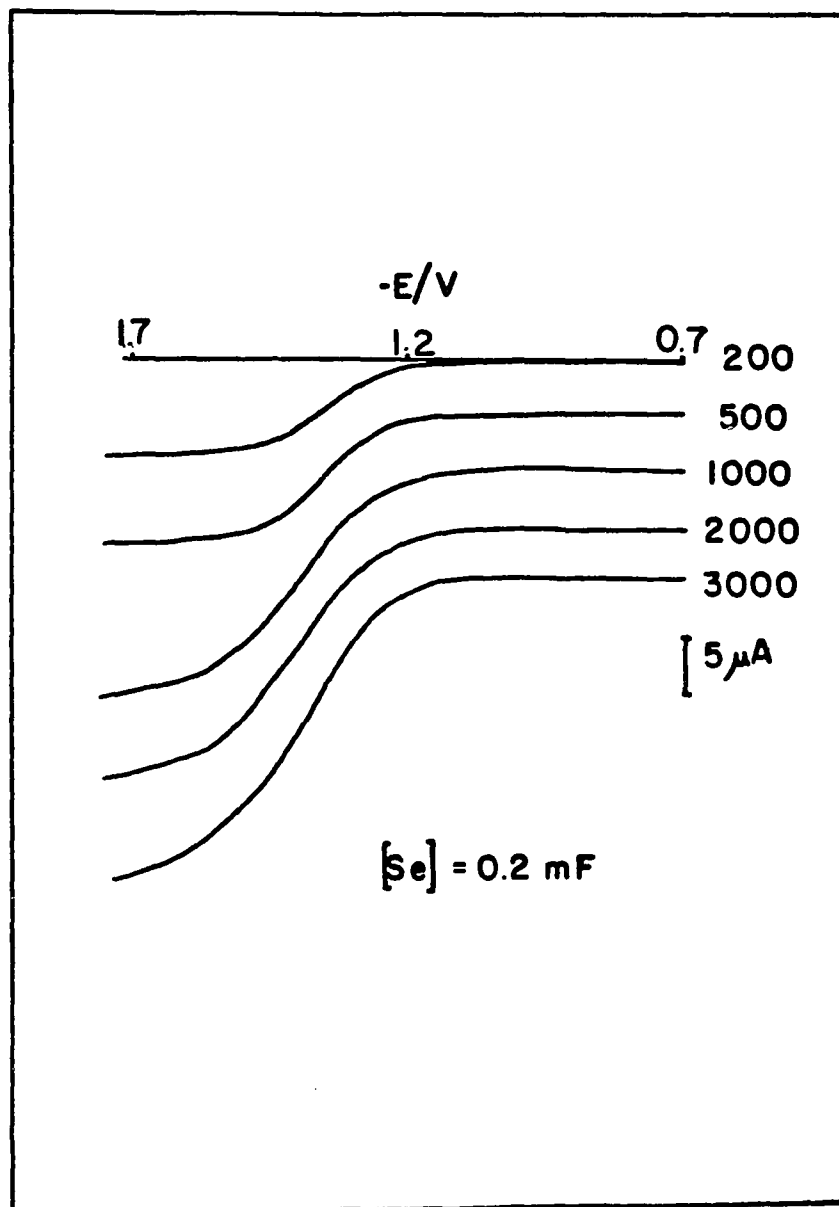
Figure 7. Reduction of Selenium at a Rotating Ring Disc
Electrode at 23° C
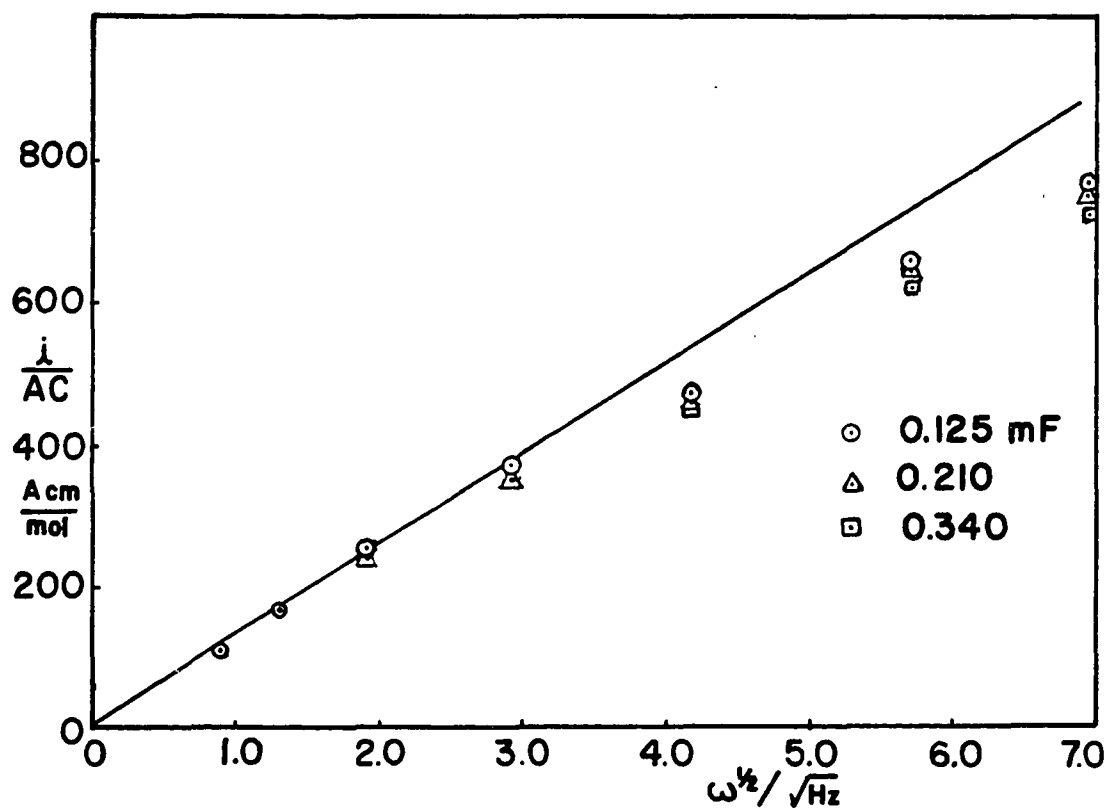
Figure 8. Effect of $\omega^{\frac{1}{2}}$ on Disc Currents for Selenium at
-1.4V at 23°C.
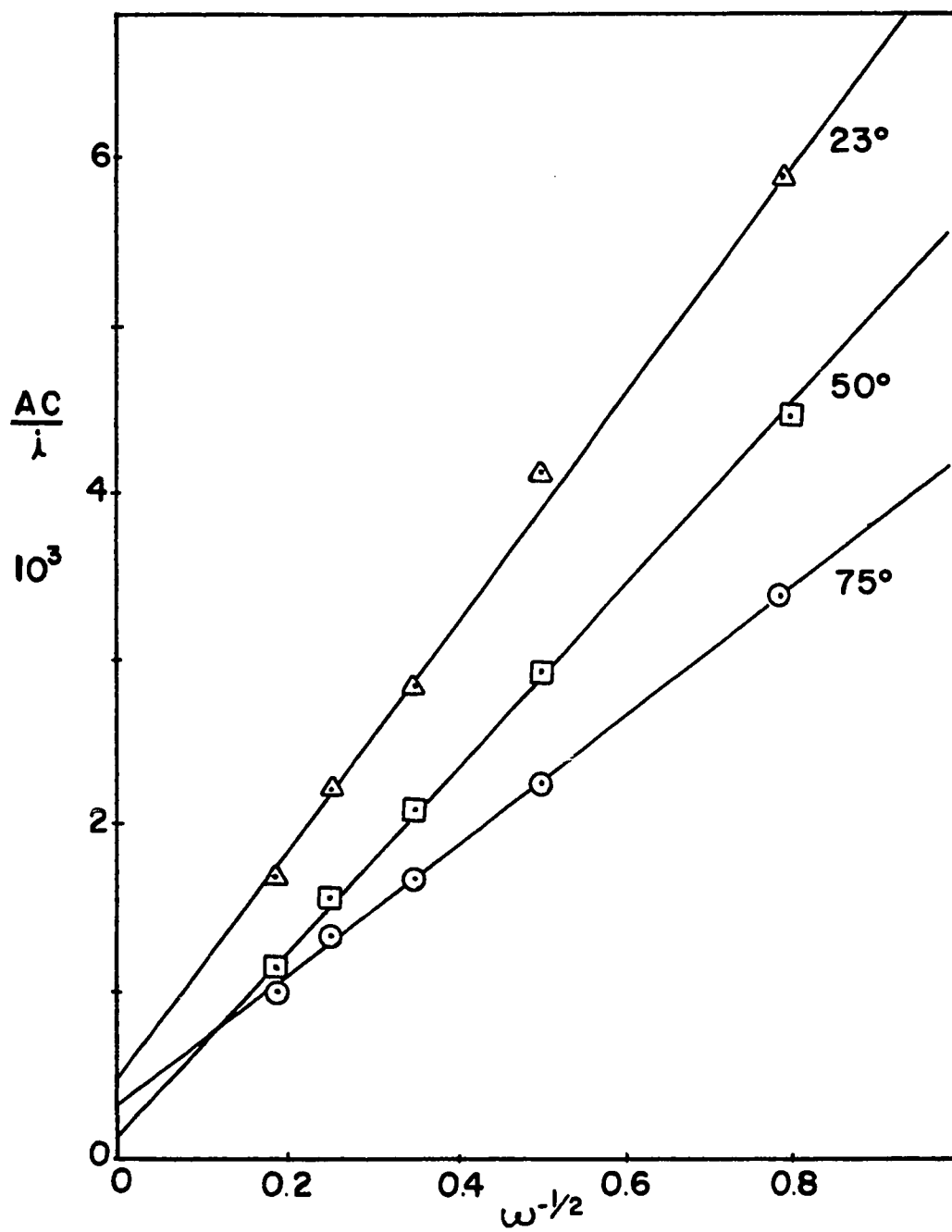
Figure 9. Temperature Effect on Disc Currents for Selenium.

TABLE I

RATE CONSTANTS FOR THE REDUCTION
OF SELENIUM

$Se_8 \times 10^5$	$i_k/AC \times 10^3$	k^o cm $\cdot$ s^{-1}
4.25	3.19	1.58×10^{-5}
2.63	3.07	7.94×10^{-5}
1.46	2.53	5.02×10^{-6}

The transfer coefficient (α) was calculated from the slope
of plots of the -log k versus -log C. for the different potentials as
shown in Figure 10. The average value was found to be 0.52 $\pm$ 0.04.

HPLC separation. Selenium in DMSO was separated by HPLC
into Se_6, Se_7, and Se_8 fractions. A typical chromatogram for the
selenium fractions is given in Figure 11. The retention times and
capacity factors (k') for each species are given in Table II.

TABLE II

HPLC SEPARATION OF SELENIUM

Species	R_t (min)	k'	log k'
Se_6	2.24	1.40	0.15
Se_7	3.04	1.90	0.28
Se_8	5.52	3.45	0.54
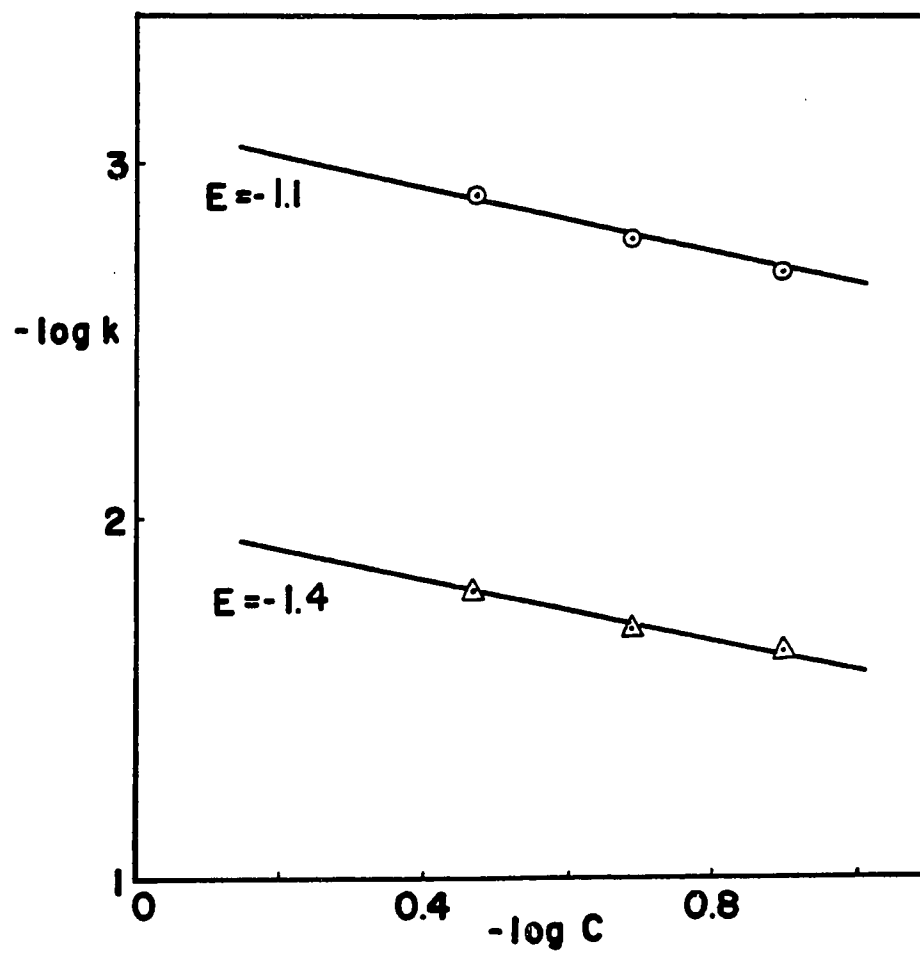
Figure 10. -Log k Vs -Log C for Selenium.
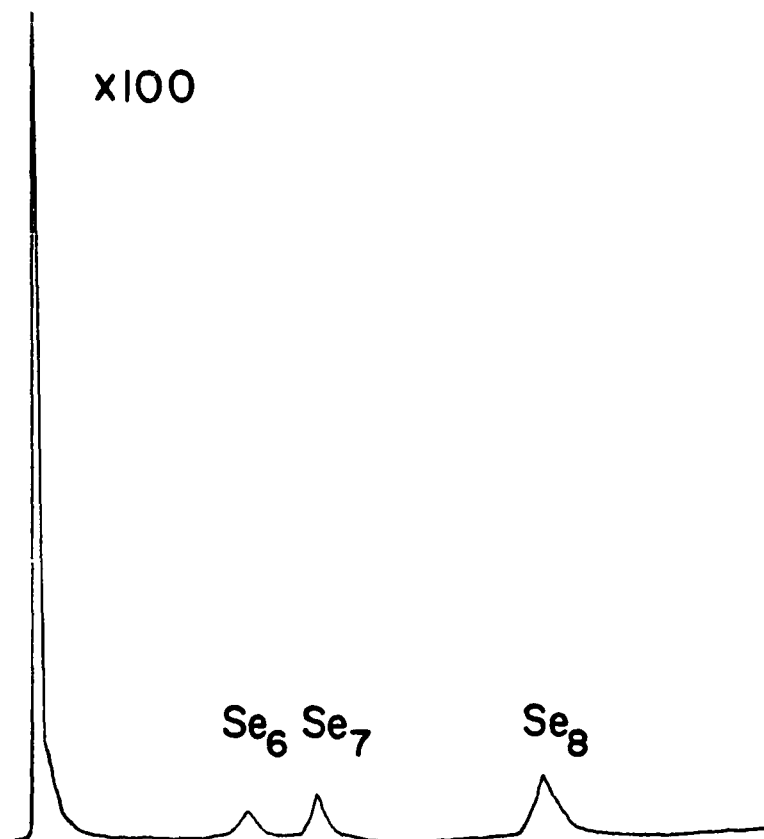
Figure 11. HPLC Separation of Selenium in DMSO.

Reaction between metallic cadmium and selenium. The reaction
was followed by HPLC, a typical chromatograph for this reaction is
given in Figure 12. Table III shows the relative amounts of
selenium before and after the reaction with cadmium.

TABLE III

REACTION OF Se_x WITH METALLIC CADMIUM

Total Cadmium mg.	Se_x	Before Reaction	After Reaction	% Change
30	Se_6	3.5×10^{-4}	1.7×10^{-4}	51
	Se_7	5.2×10^{-4}	2.2×10^{-4}	58
	Se_8	7.8×10^{-4}	4.2×10^{-4}	46
50	Se_6	3.5×10^{-4}	1.3×10^{-4}	63
	Se_7	5.2×10^{-4}	1.7×10^{-4}	67
	Se_8	7.8×10^{-4}	3.0×10^{-4}	62
100	Se_6	3.5×10^{-4}	0	100
	Se_7	5.2×10^{-4}	0	100
	Se_8	7.8×10^{-4}	1.7×10^{-5}	98
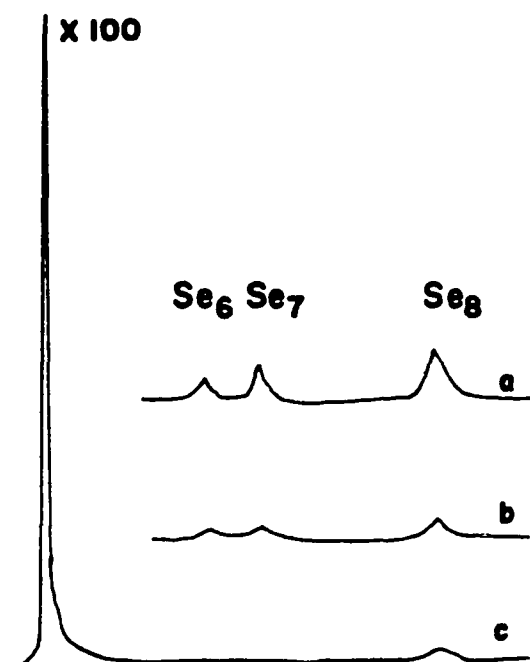
Figure 12. HPLC Chromatograms of a Saturated Selenium
Solution a) Before Reaction b), c) After
Reaction with 50 and 100 mg of Metallic Cadmium.

Sulfur

Electrochemistry. Current voltage curves for the reduction of
sulfur over the potential range of 0.0 to -1.0V versus Ag/AgCl, at
rotation rates of 200 to 4000 rpm, concentration range of 0.10 to
0.75 mF and temperatures of 23 to 100°C were recorded. A typical
run for a given concentration and at room temperature for the disc
is given in Figure 13.

Results covering the concentration range are summarized in
Figure 14 for the normalized current at -0.8 V. All of these plots
have curvature, increasing at very high rotation rates. Separation
of diffusion and kinetic contribution to the total current are shown
by reciprocal lpots in Figure 15 for several potentials and in Figure
16 for several temperatures.

The diffusion coefficient (D) for S_8 in DMSO was calculated
from the slope of the plots of Figure 16 according to equation 1.
The diffusion coefficient follows expression 14 for the range of
temperatures 23 - 100°C, where T is in kelvin.

$$\log D = - 910.75 \left(\frac{1}{T}\right) - 2.31 \qquad\qquad 14$$

At 25°C D was equal to 1.95 x 10^{-6} $cm^2 s^1$

Kinetic currents were also determined from Figures 15 and 16.
The plot was fitted by a least squares method and extrapolated to
$w^{-\frac{1}{2}}$ = 0. A summary of the kinetic current values is given in Table IV.

TABLE IV

INTERCEPT VALUES OF $(\frac{AC}{i})$ FOR SULFUR REDUCTION $\times 10^3$

mF	23°	50°	75°
0.10	0.299 ± 0.089	0.278 ± 0.048	0.220 ± 0.021
0.20	0.375 ± 0.102	0.229 ± 0.031	0.186 ± 0.031
0.40	0.420 ± 0.089	0.278 ± 0.039	0.200 ± 0.017
0.75	0.414 ± 0.061	0.285 ± 0.055	0.202 ± 0.032

The reaction rate constant was calculated from i_k and equation 11. Average rate constants are given in Table V. The transfer coefficient (α) was calculated from a plot of $-\log k$ versus $-\log C$ for the different potentials as shown in Figure 17. Rate constants at $-0.8\,V$ at several temperatures are summarized in Table V.

TABLE V

HETEROGENEOUS RATE CONSTANTS FOR THE REDUCTION OF SULFUR

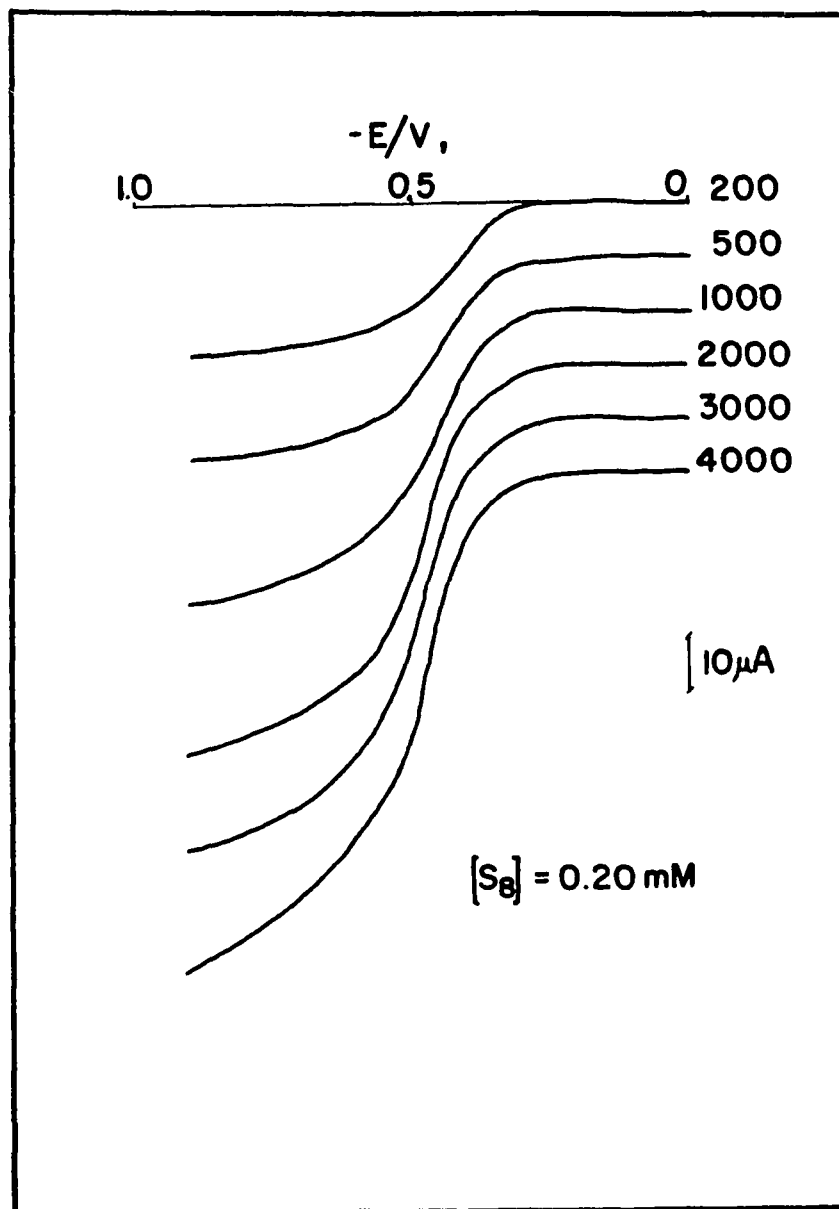| $^{\circ}C$	$k^{\circ} \; cm \cdot s^{-1}$
25	$3.31 \pm 0.04 \times 10^{-4}$
50	$5.47 \pm 0.11 \times 10^{-4}$
75	$7.32 \pm 0.12 \times 10^{-4}$

Figure 13.   Reduction of Sulfur at a Rotating Ring-Disc Electrode.
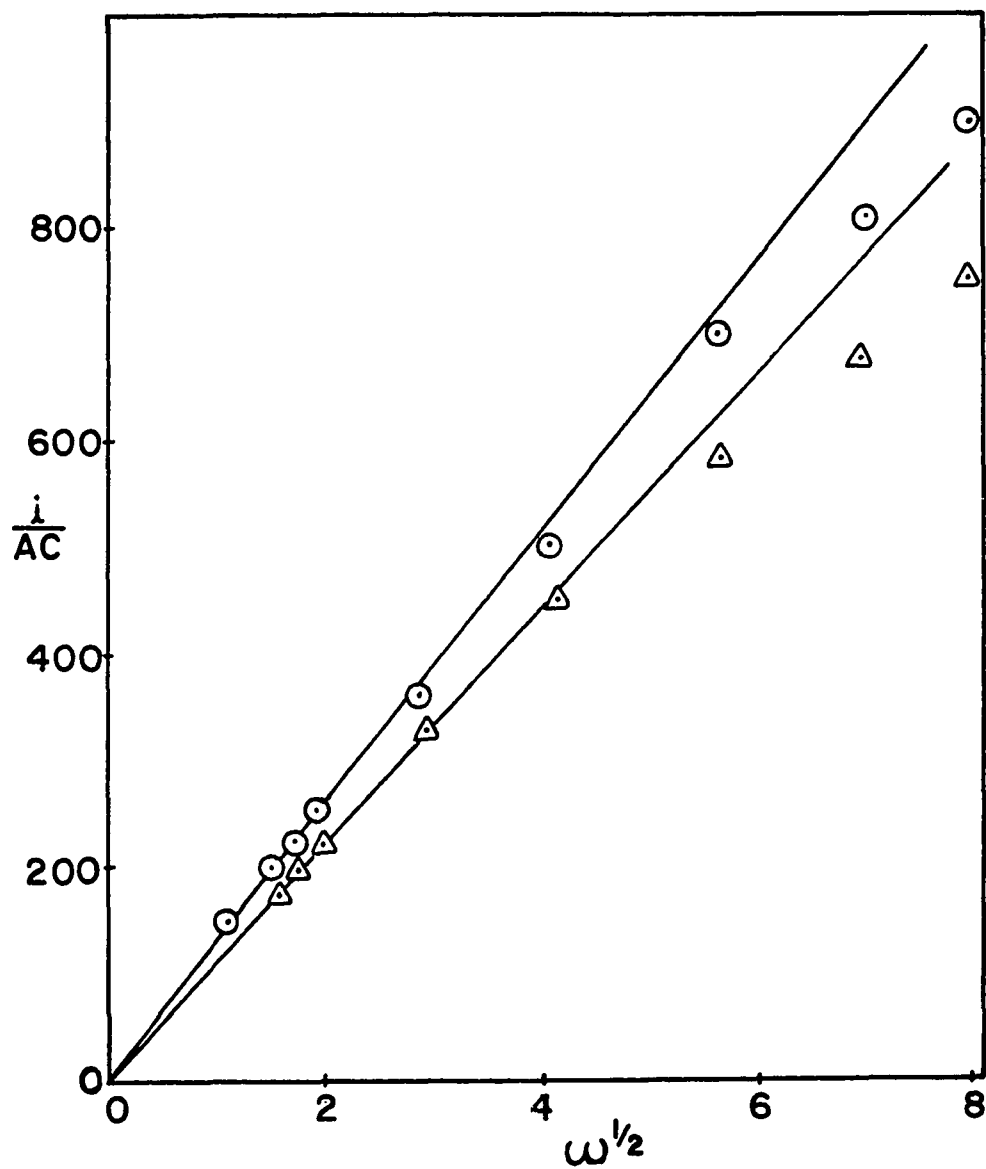
Figure 14. Effect of $w^{1/2}$ on Disc Current i_D for S_8 at $23^\circ C$.
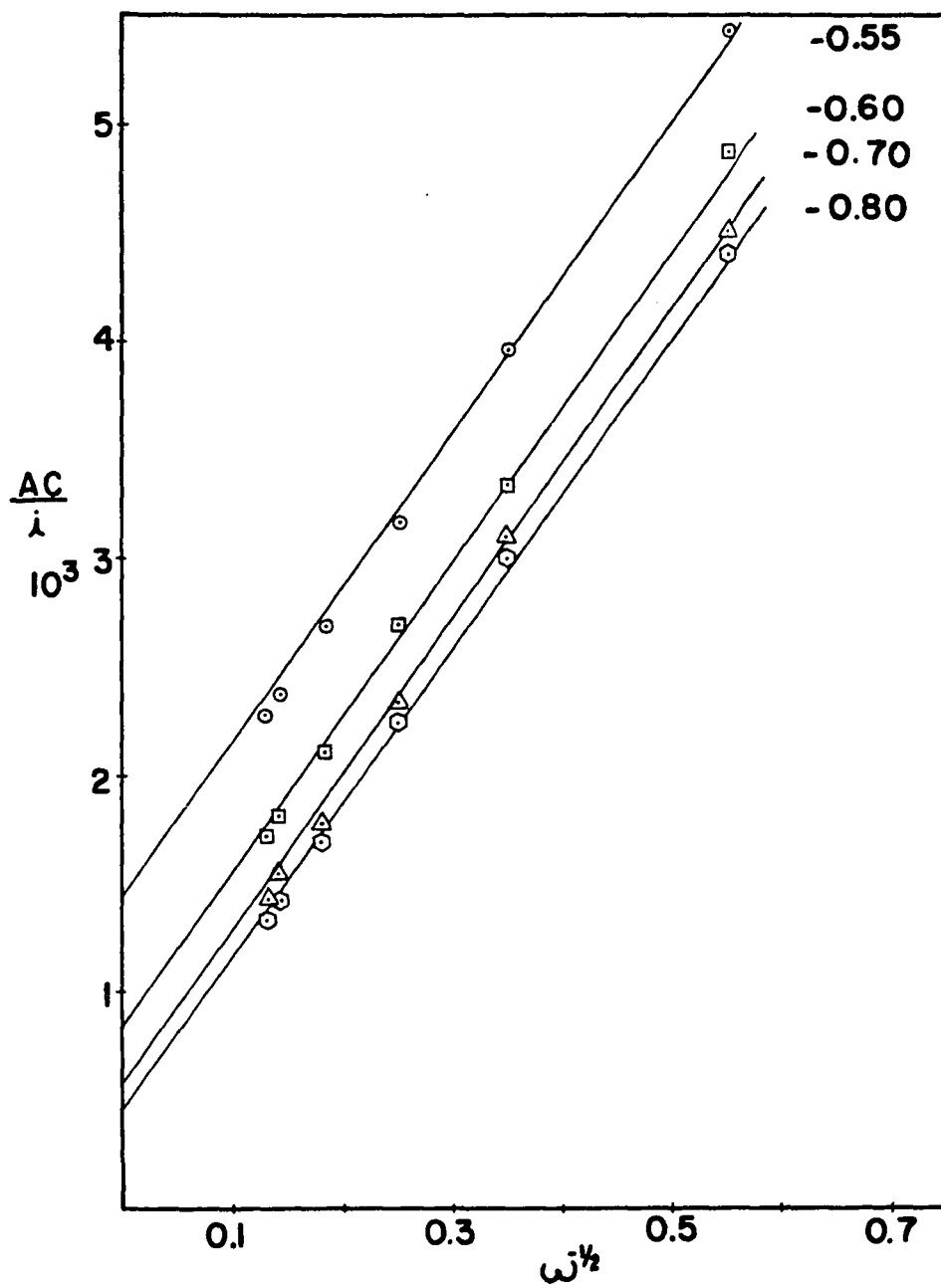
Figure 15. Effect of the Disc Potentials on the Kinetic Currents
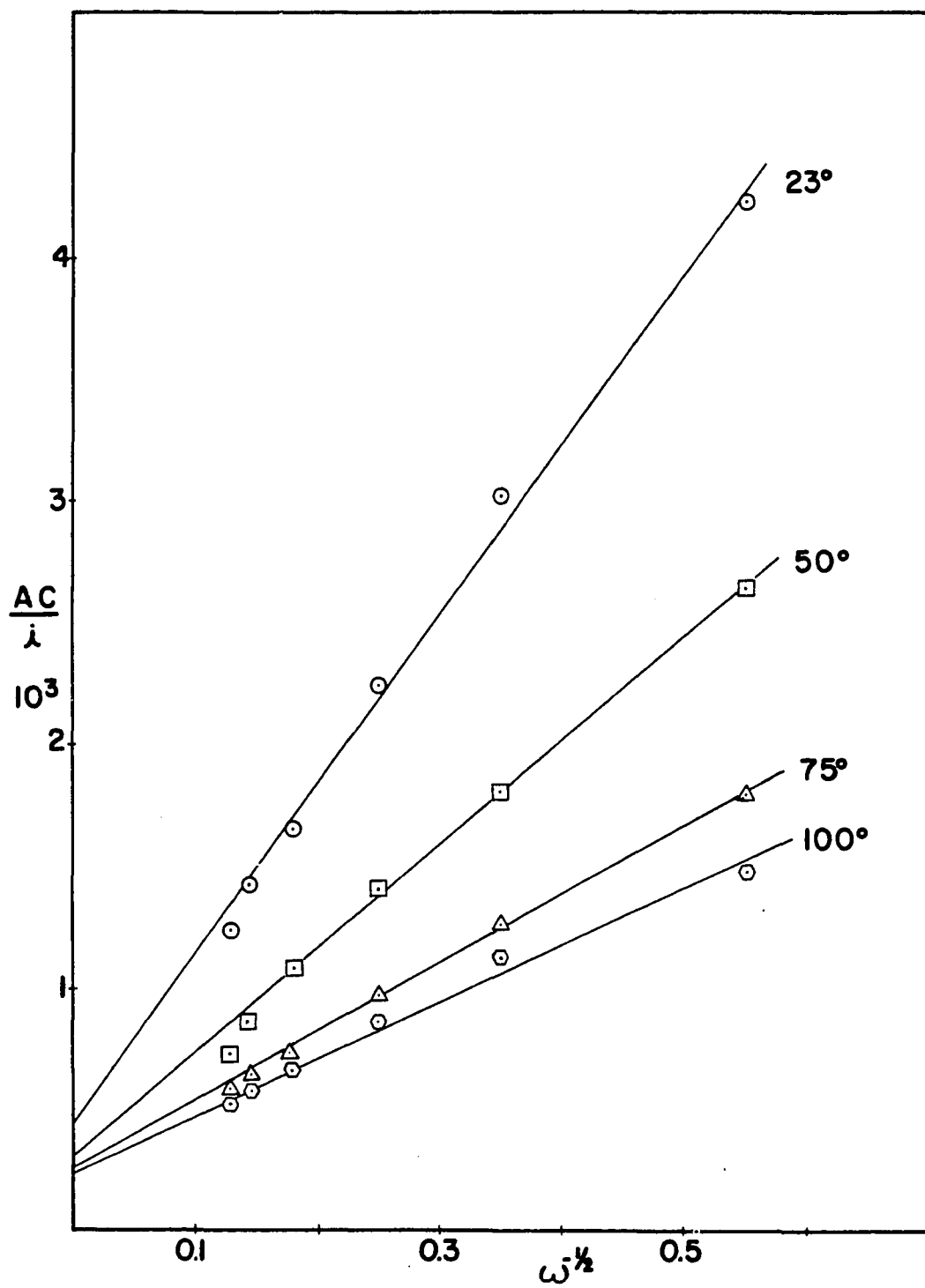
Figure 16. Temperature Effect on $(1/AC)^{-1}$ for S_8.

<u>Ring measurements of products during the reduction of sulfur</u>.
The ring electrode was scanned in search of products from +0.7 to
-1.0 V while the disc electrode was kept at -0.8V during the reduc-
tion of S_8 to S_8^{-2}. A typical scan is shown in Figure 18. At 23°
ring current measured at +0.4V versus Ag/AgCl agree with those
calculated from the collection efficiency (see Figure 19).

As the temperature was increased the solution changed color
from clear to a light blue-green and the ring electrode scans did
not show as steep a rise and ring currents were approximately 50%
lower than those predicted from the collection efficiency (Figure 18).

An apparent reaction between the produced polysulfides and
oxygen was suspected since ring currents decreased with time. A
new set of experiments in a glove bag filled with nitrogen were
conducted to test this possibility. Disc-ring currents improved
only by $\sim$ 3%, indicating that oxygen was not responsible for the
decrease in currents, but instead a slow reaction with the gold
electrode may be occurring since a brown film was found on the
electrode surface.

<u>HPLC separation</u>. Sulfur in DMSO solutions were separated into
fractions of S_6, S_7, and S_8. A typical chromatogram of this separ-
ation is shown in Figure 20. The retention times (R_t) and capacity
factors (k') are given in Table VI.
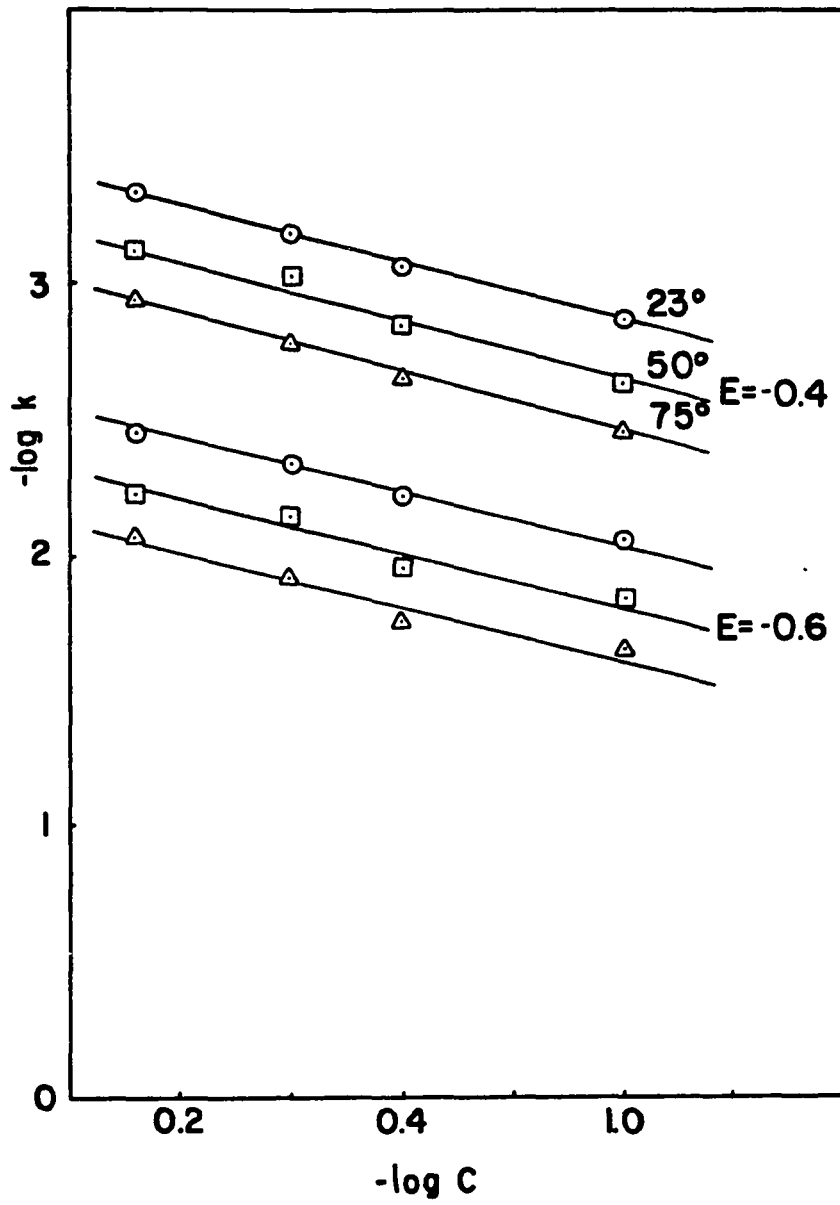
Figure 17. -Log k versus -Log C for the Reduction of Sulfur.
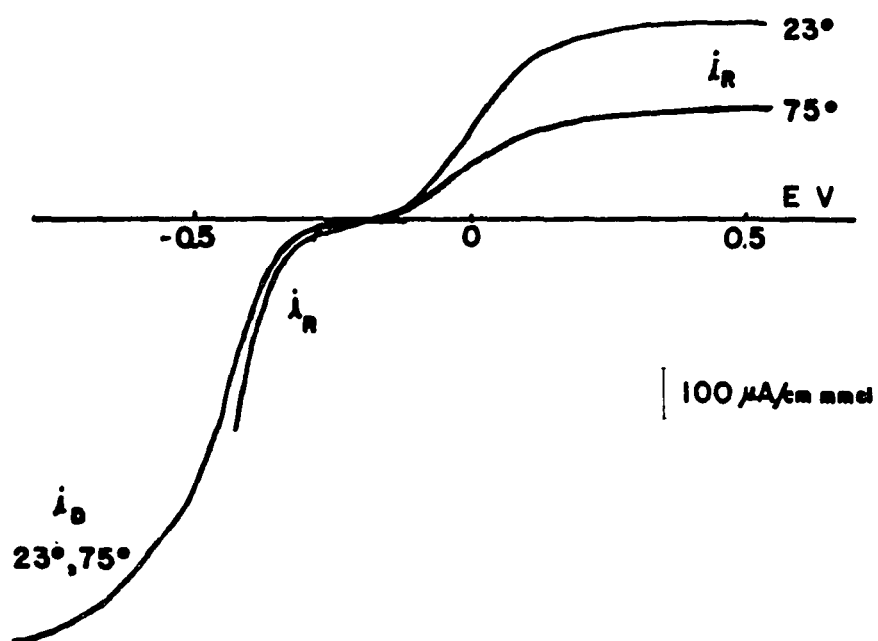
Figure 18. Ring Scans During the Reduction of Sulfur at the Disc Electrode at 23° and 75°C.
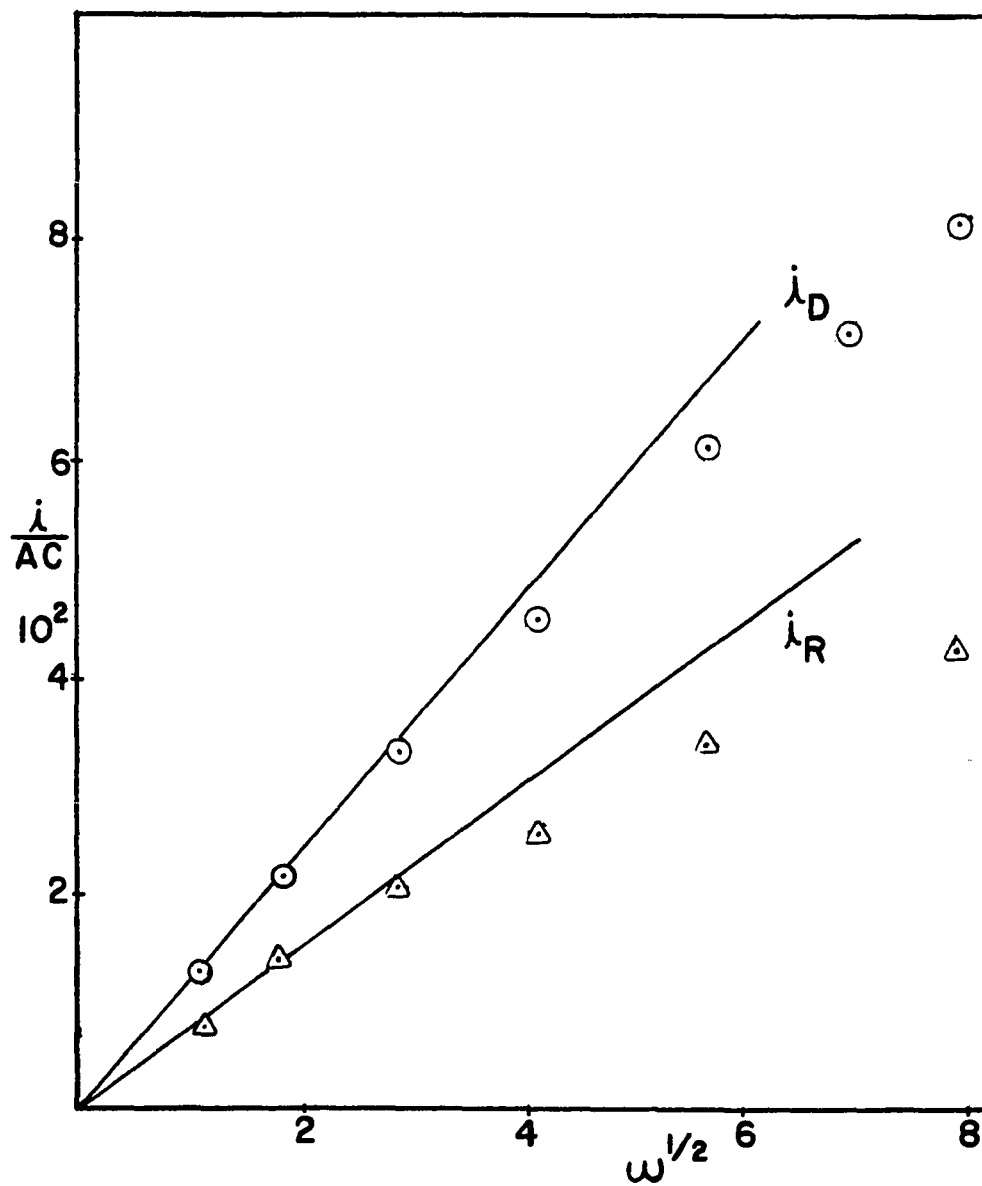
Figure 19. Effect of $w^{\frac{1}{2}}$ on Disc and Ring Currents for Sulfur at $23^{\circ}C$.

TABLE VI

HPLC SEPARATION OF SULFUR IN DMSO

Species	R_t (min)	k'
S_6	1.88	0.96
S_7	2.52	1.29
S_8	3.96	2.02
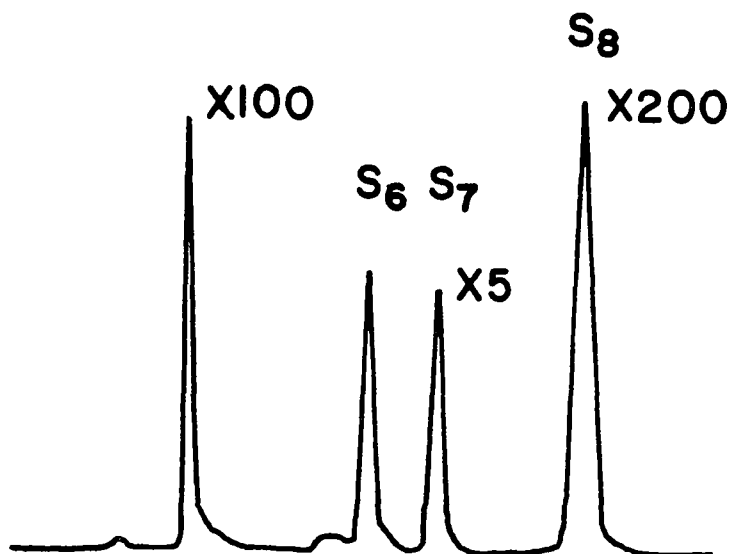
Figure 20. HPLC Separation of Sulfur in DMSO.

The UV absorbance spectrum for S_6, S_7, and S_8 were constructed from the chromatogram recorded from the range of 250 to 300 nm. The spectra are shown in Figure 21. The spectrum for total sulfur was constructed from the summation of different spectra.

Electrochemistry of S_6, S_7, and S_8. Fractions of S_6, S_7, and S_8 were collected and the electrochemistry of each fraction studied by cyclic voltammetry using a gold microelectrode. Little information was obtained from cyclic voltammetry because of the low concentration of S_6 and S_7.

Further studies of the electrochemistry of the sulfur fractions were conducted using the flow cell for the potential range from -0.35 to -1.60 V versus Ag/AgCl. These electrochemical studies showed that the S_6 and S_7 fractions are not reduced at the potential range possible, but instead they show small anodic currents as shown in Figure 22. The reduction current-voltage curve for the S_8 fraction was reconstructed for the potential range studied, and it is shown in Figure 23.
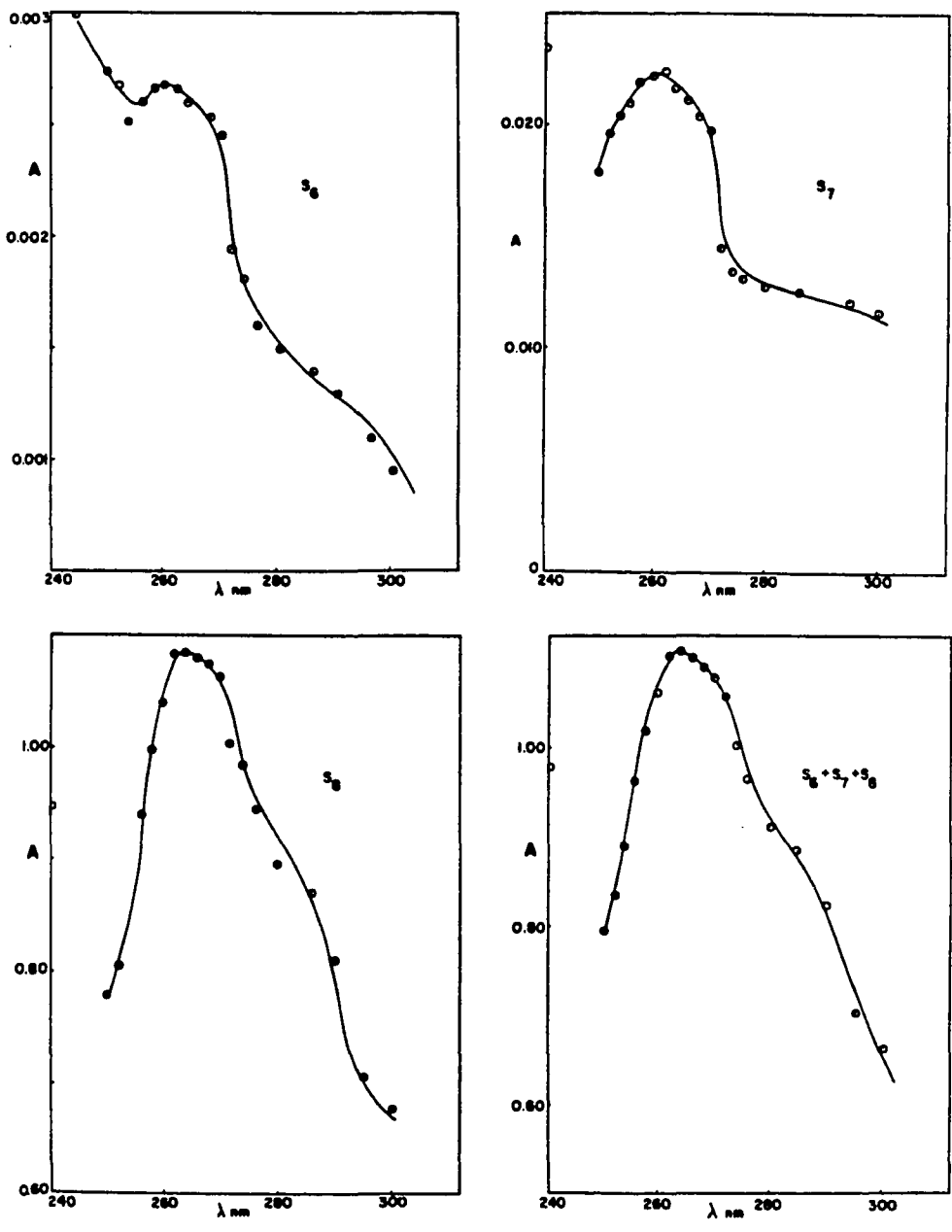
Figure 21. UV Spectra for S_6, S_7, and S_8 from HPLC Data.
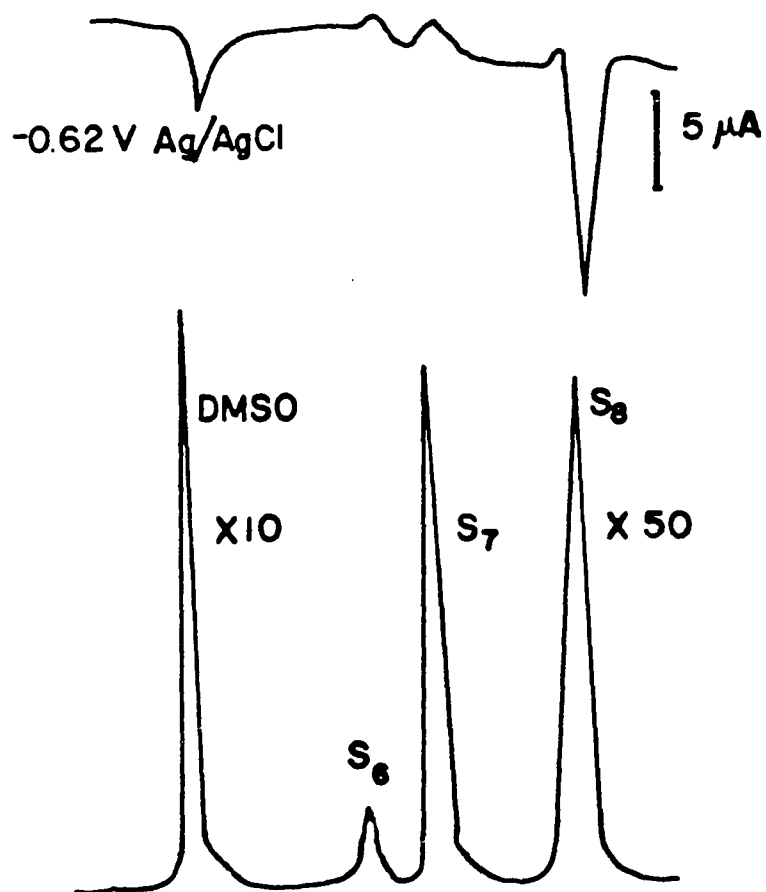
Figure 22. Current-Time Curve for S_6, S_7, and S_8 in a Flow Cell Compared to the UV Detector Response.
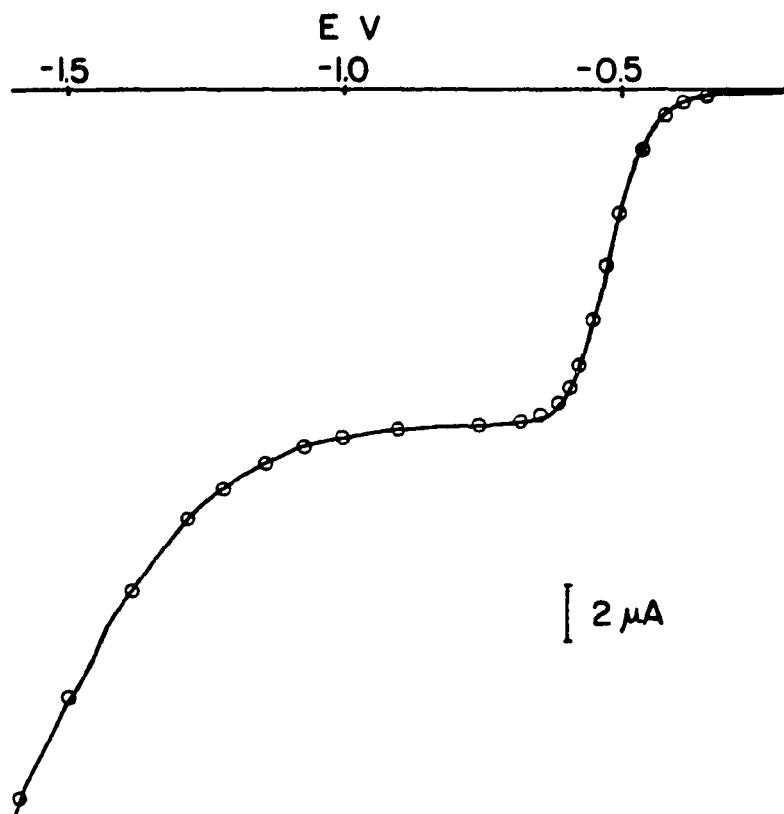
Figure 23. Current-Voltage Curve for the Reduction of S_8 in a
Flow Cell.

Reaction of S_x with metallic cadmium. Freshly precipitated
cadmium was reacted with sulfur in DMSO and the reaction followed by
HPLC. Typical chromatograms of reactant and product solutions are
given in Figure 24. The relative amounts of sulfur before and
after the reaction are given in Table VII.

TABLE VII

REACTION OF S_x WITH METALLIC CADMIUM

Total Sulfur	S_x	Before rxn	After rxn	% Change
0.5 mF	S_6	0.0021	0.0010	48
	S_7	0.0017	0.0015	91
	S_8	1.0500	0.9000	14
1.0 mF	S_6	0.0055	0.0032	41
	S_7	0.0033	0.0050	85
	S_8	2.0700	1.7700	14
2.5 mF	S_6	0.028	0.013	54
	S_7	0.180	0.056	67
	S_8	3.800	3.420	10
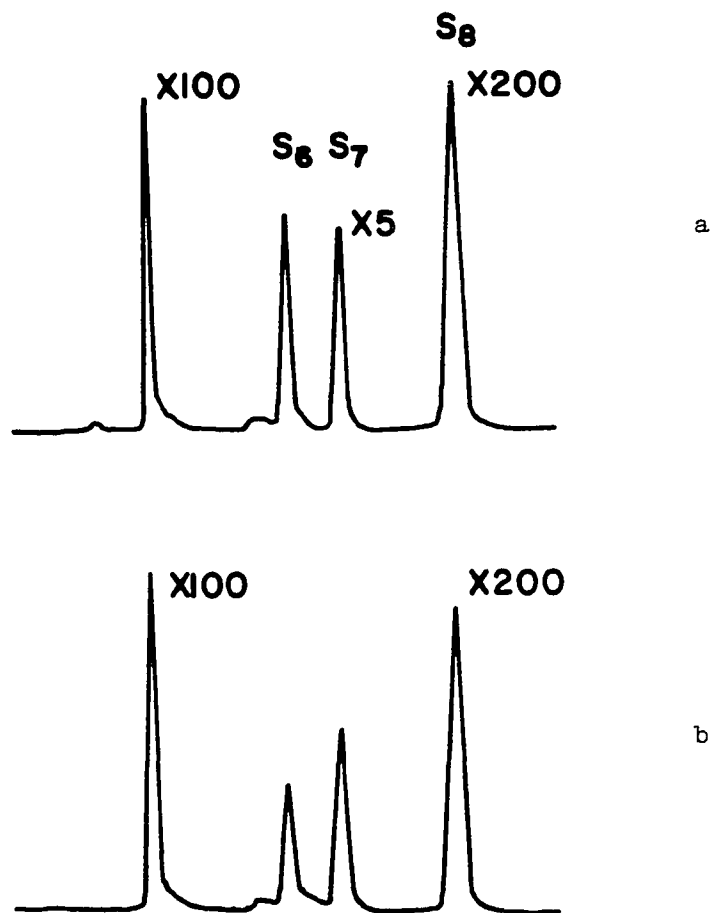
Figure 24. HPLC Chromatogram for the Reaction of Sulfur with
            Cadmium, (a) Before Reaction and (b) After Reaction.

<u>Cadmium</u>

<u>Electrochemistry</u>. Cadmium (II) in DMSO was reduced at a gold microelectrode and at a RRDE. The reduction is well behaved and shows a characteristic underpotential deposition region at - 0.45 V versus Ag/AgCl. Bulk deposition of cadmium starts at -0.5 V. The anodic peak for the reoxidation of the cadmium monolayer appears at 0.0 V. A typical current voltage curve for the reduction is shown in Figure 25. The diffussion coefficient was calculated to be 1.92×10^{-6} cm^2 from the plot i_D/AC versus $w^{\frac{1}{2}}$ in Figure 26.

The rate constants for the formation of the cadmium deposits were calculated from the kinetic currents, the results are given in Table VIII.

TABLE VIII

HETEROGENEOUS RATE CONSTANTS FOR THE REDUCTION OF CADMIUM

Temperature C	D cm^2sec^{-1}	$k_{-0.5V}$ cm sec^{-1}
23	1.92×10^{-6}	0.0605
50	2.66×10^{-6}	0.0693
75	2.86×10^{-6}	0.0790

<u>Electrochemical formation of cadmium sulfide and selenide</u>. Electrochemically deposited cadmium was reacted with selenium at potentials close to the underpotential deposition of cadmium. A shift in the anodic peak of cadmium towards more positive poten-
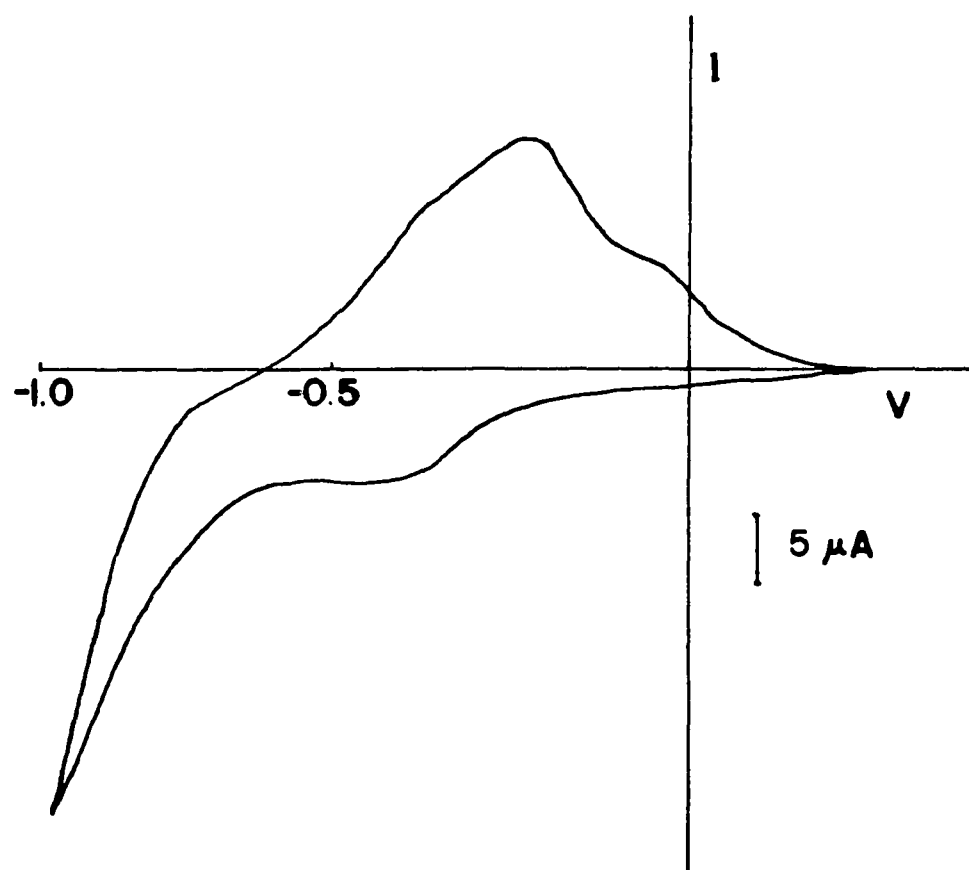
Figure 25. Reduction of Cd (II) at a RRDE at 1000 rpm.
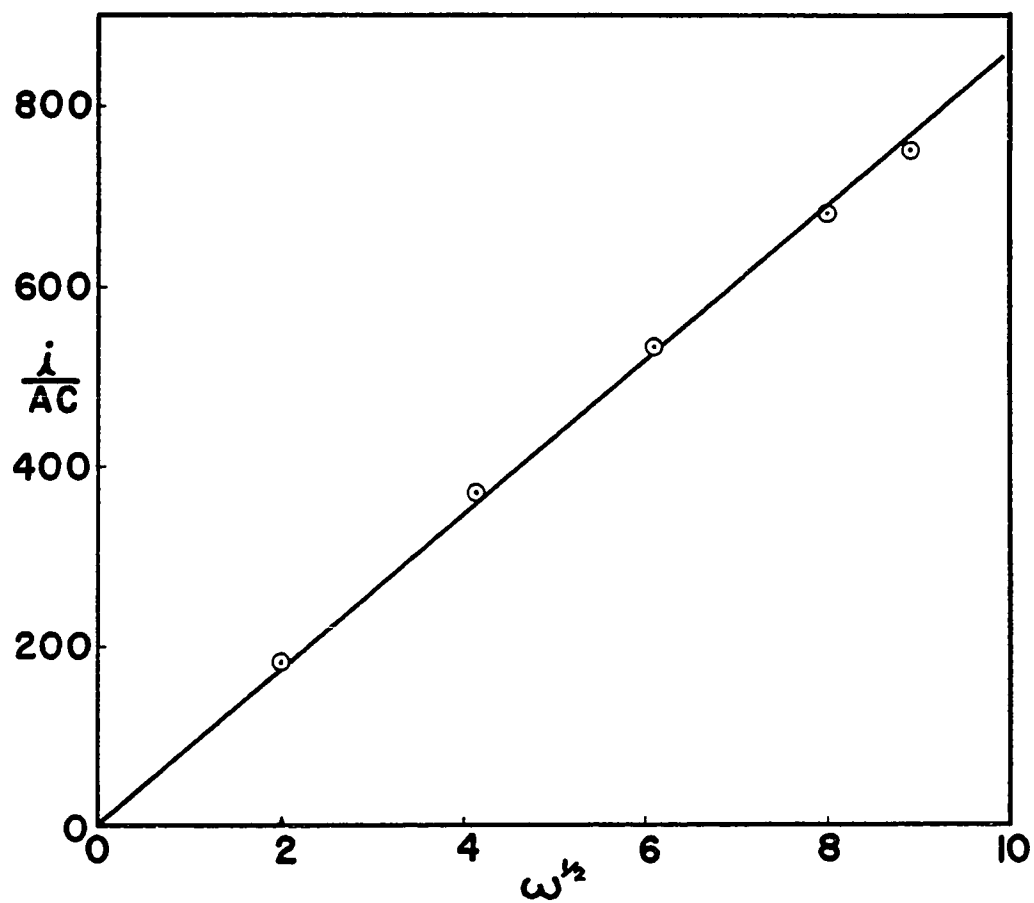
Figure 26. Effect of $w^{\frac{1}{2}}$ on Disc Current i for Cadmium at 23°C.

tials was observed while the cathodic peak increase markedly in
magnitude. A typical current-voltage curve for this reaction is
shown in Figure 27. As larger concentrations of selenium reacts
with cadmium, the anodic peak shifts and levels off after all the
cadmium has reacted, as seen in Figure 28. The total anodic
charge for the striping of the cadmium selenide from the electrode
surface also level off indicating the total reaction of the
cadmium as shown in Figure 29.

Measurements with the ring electrode at potentials of +0.1
and +0.2V shows a single soluble product (Figure 30). The concen-
tration of this soluble product decays in the region of the under-
potential deposition of cadmium. The observed ring currents, however,
are only 20% of the expected currents.
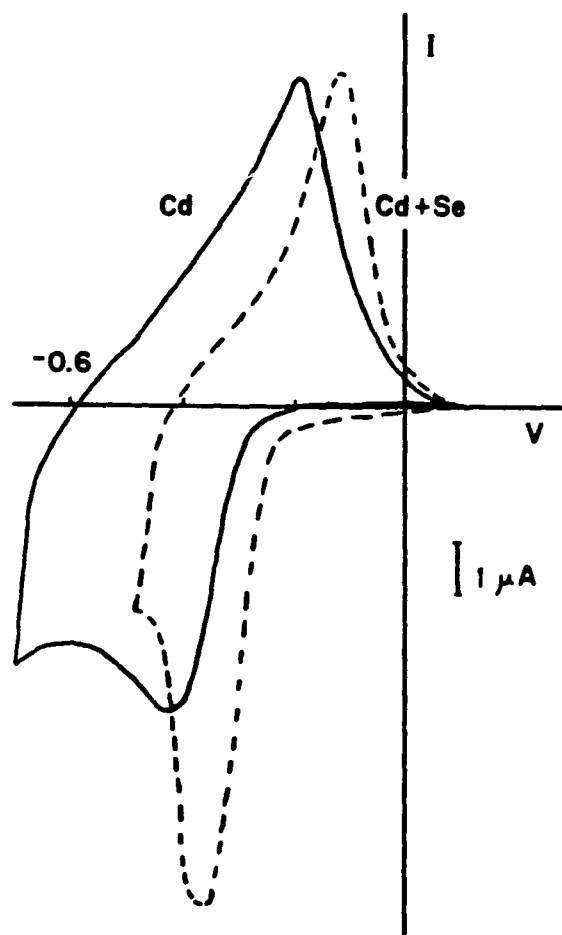
Figure 27. Electrochemical Formation of CdSe.
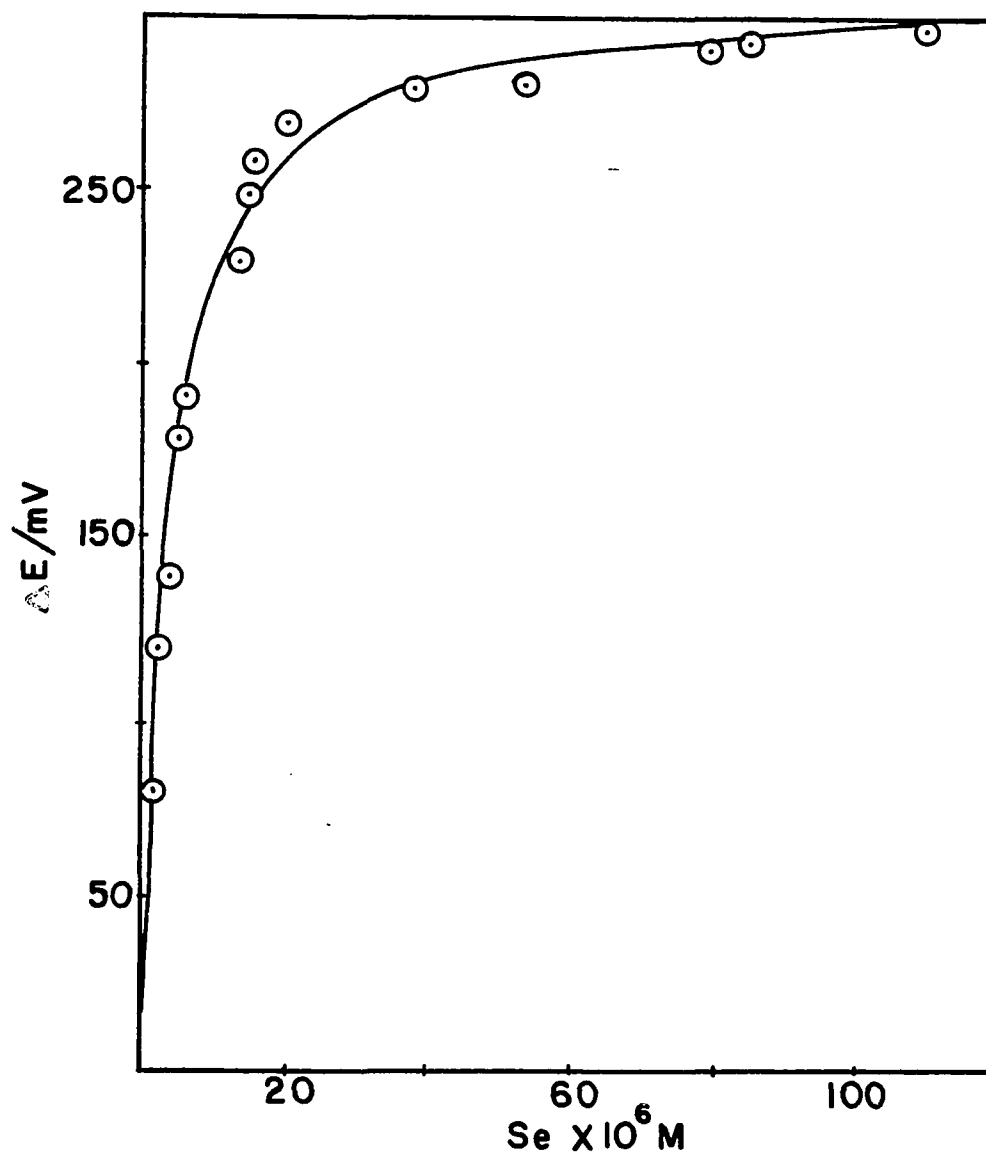
Figure 28. Potential Shift on the Anodic Peak of Cadmium upon
Addition of Selenium.
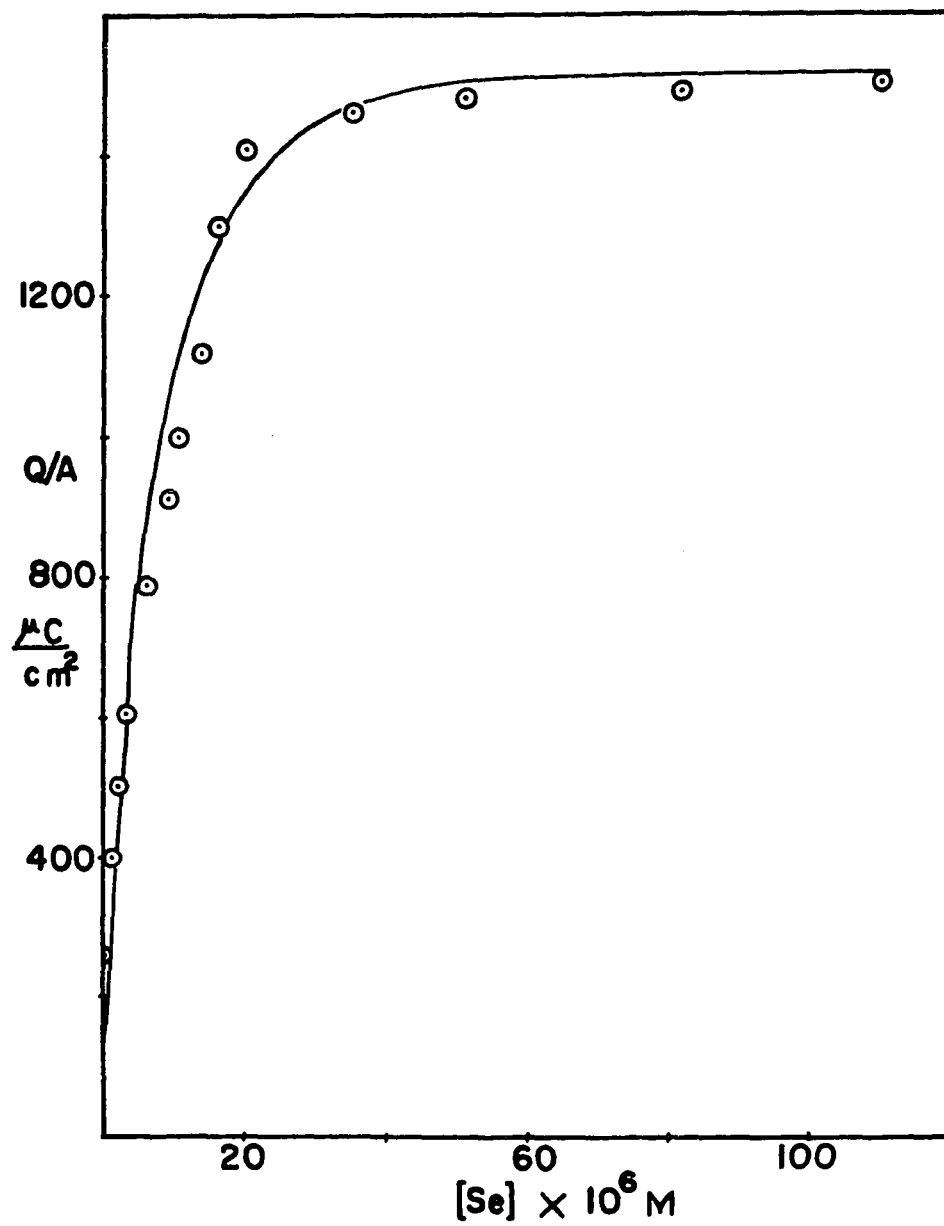
Figure 29. Total Charge in the Stripping of CdS as a Function of Selenium Concentration.
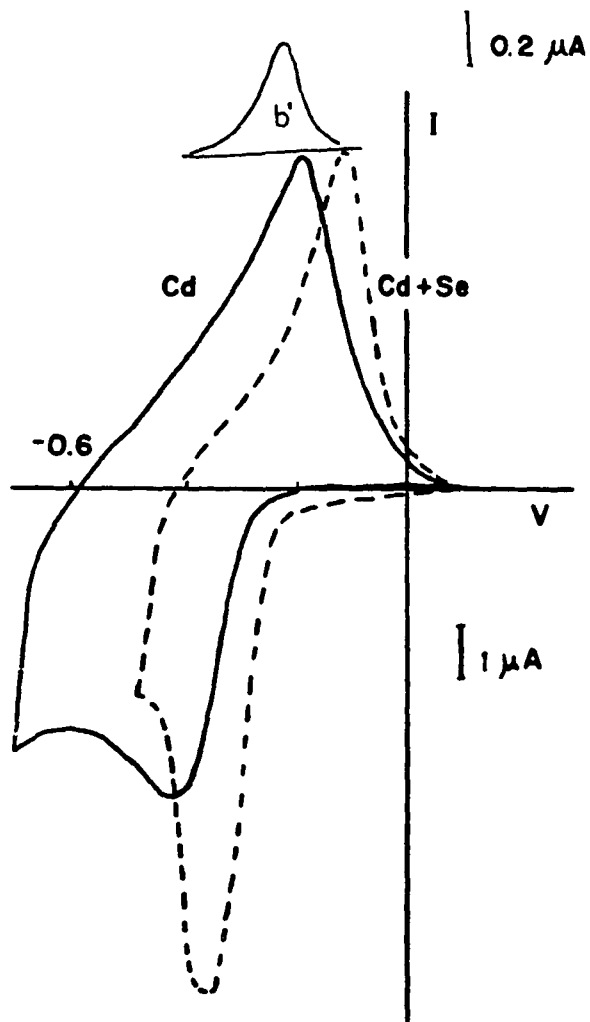
Figure 30. Soluble Products (b') at the Ring Electrode
during the Electrochemical Deposition of
CdSe at the Disc.

CHAPTER IV

DISCUSSION

Electrochemical techniques, HPLC, and UV spectroscopy were used
to determine the mechanism of the reaction involved in the electro-
chemical deposition of CdS and CdSe. The overall mechanism was
originally proposed by Baranski (31) and Roe (30). From the over-
all mechanism (eqns. 1, 2a, 2b, 3a, and 3b) a number of elementary
reactions as well as side reactions can also occur. The rates of
these side reactions will determine their contribution to achieve
our goal of producing thin films of controlled stoichiometry,
crystallinity and semiconducting properties. The elementary steps
studied for these reactions include the kinetics of the electro-
chemical reduction of cadmium ions, sulfur and selenium molecules,
all at a gold RRDE in DMSO solution over a wide range of temperatures
and concentrations. Standard heterogeneous rate constants (k°) for
the reduction of sulfur and selenium have also been estimated.

Kinetics of the reduction of cadmium ions from DMSO solution at
a gold electrode have not been previously reported. At a DME (55),
reduction of Cd(II) appeared to be diffusion controlled. However,
the reaction at a gold surface is strongly influenced by surface
process. Deposition of cadmium ion from DMSO at a gold RRDE and at
a gold microelectrode presented a broad reduction wave in the under-
potential deposition region rather than the narrow peak reported by

Kolb, et al (50) in aqueous solutions. This is probably due to the surface preparation rather than the solvent. The development of the underdeposition potential region suggests the slow restructuring of the gold. Our results of the reduction of cadmium at potentials just negative of the underpotential deposition region showed that this process is very fast (k_f = 0.06 cm s^{-1}) indicating that charge transfer to Cd(II) is not expected to inhibit the rate of the overall process of deposition of CdS and CdSe.

It has been noted (30) that on a CdS surface, deposition of Cd(II) has a considerable overpotential compared to deposition on gold or cadmium. There are two reasons for this: nucleation and resistance of the CdS film. Once the nucleation barrier is overcome further deposition proceeds rather rapidly. The presence of sulfur helps to decrease the nucleation potential (30).

Selenium presents very similar results to those of sulfur. Effects on the underpotential region of cadmium due to the presence of selenium were evident even at a Se/Cd ratio of 0.00125 in RRDE measurements. A positive shift up to 300 mV (Figure 28) in the anodic peak was observed when selenium was added, while the cathodic peak showed a shift not larger than 40 mV. Ratios of Se/Cd higher than 0.1 did not shift the anodic peak any further.

The reoxidation of a single soluble product was observed at the ring (E_r = +0.4) when the selenium and cadmium reacted (see Figure 30). This stable intermediate is perhaps due to the oxidation of polyselenides and possibly also dissolved CdSe and its complexes. A similar product was reported (30) during the formation of CdS.

Electrochemical characteristics of sulfur, as well as selenium in DMSO are in sharp contrast to that of cadmium. One of the most unusual observations is that from the three sulfur rings present in solution, S_6, S_7, and S_8, only S_8 is reducible at a gold electrode while S_6 and S_7 appear to absorb strongly on the electrode surface. HPLC separation of these and higher rings compounds has been documented by two research groups (40, 41) using a UV absorbance detector. However, electrochemical detectors have not been previously used with sulfur or selenium. Figure 22 shows the response of the UV and electrochemical detectors in series showing unequivocally the lack of electrochemical response of S_6 and S_7 on a gold electrode. A complete current potential curve for S_8 was compiled from a series of individual injections and a series of potentials. A comparison of the results in Figure 23 with the RRDE curves of sulfur in DMSO, as shown in Figure 13, indicates without a doubt that S_8 is the species that is responsible.

Electrochemical studies reported in the literature (48, 49) as well as those reported in the experimental section refer to S_8 which is of course, the major species present in solution. Although small, perhaps depending on the method of preparation of the solution, variable amounts of S_6 and S_7 are usually present (40). Therefore it is customary to identify sulfur solutions as consisting of S_8 molecules and hence to calculate the concentration on the basis of this molecule. Even though S_8 certainly determines the observed electrochemical behavior, such as reduction potential and rate of charge transfer, it is also interesting to propose what the role of S_6 and S_7 might be.

There are two experimental observations that are relevant to the electrochemical role of S_6 and S_7. First it was noted that cathodic currents decrease with successive scans. This decrease was not caused by oxygen diffusing into the solution and reacting with the products, although the reaction products are sensitive to oxygen. Periodic cleaning of the gold electrode was needed to obtain reproducible results, especially at elevated temperatures. This cleaning operation could be accomplished by applying a positive potential or by removing the electrode and polishing with fine alumina. A definite surface reaction occurred since a brown film was formed on the electrode surface.

To verify if the decrease in current was indeed due to a kinetic process or not, the electrode was repolished and the high rotation rate measurements were made first. The observed currents were lower than those expected, indicating that indeed the decrease was due to a kinetic process and not to film formation.

Secondly, from the HPLC chromatograms S_6 and S_7 are not reduced but instead the current-time curve shows anodic peaks at all potentials from -0.5 to $-1.6V$. These observations suggest that S_6 and S_7 react with a gold surface to produce a very stable absorbed layer or surface compound. Gold is negatively charged relative to the solution in the potential range studied, and the formation of a surface compound that involves no apparent net current for its formation can cause an external current by a change in the double layer structure. That is, formation of a Au-S layer causes the reorientation of the dipoles (methanol molecules in the HPLC experiment) and change in the ionic

composition of the outer Helmholtz plane.

Barlett (56), some years ago, and recently others (57) noted that S_6 and S_7 are much more reactive than S_8 in some homogeneous reactions. In a sense this is also true for the electrochemical behavior, not in terms of reduction but in terms of surface absorption.

The spectrum of S saturated vapor recorded below 250° by Bass (52) consist of unresolved maxima at 210, 265, and 285 nm. This compares well with the absorption spectrum of S_8 in nonpolar solvents, as well as in DMSO at $25^{\circ}C$. Furthermore, the spectrum is in agreement with the spectrum reconstructed from HPLC data. The S_6 and S_7 spectra were constructed from the absorbance of the S_6 and S_7 fractions from HPLC. The S_6 spectra show a resolved shoulder at 260 nm. Previous studies (53) in ethyl ether at $25^{\circ}C$ did not show a resolved peak. The S_7 spectrum has not been reported in the literature. Molar absorptivity coefficients were not calculated because no information on the concentrations of S_6 and S_7 was available from the experiment.

S_8 showed two well defined reduction waves at (-0.6, -1.1V versus Ag/AgCl) at a RRDE and at a gold microelectrode for concentrations under saturation. These results are consistent with similar studies previously reported for nonaqueous solution (36, 47-49). The first reduction wave of sulfur showed some curvature (Figure 15) for plots of i_D versus $w^{\frac{1}{2}}$ at the RRDE, which suggests some kinetic complication. Bonaterre (36) has also suggested this behavior. Paris and Plichon (49) reported that there are no kinetic complications but, their studies covered only a small rotation rate range. The

observed standard heterogeneous rate constants for the reaction given in Table V indicate moderate charge transfer rates for the temperatures studied. The transfer coefficient was equal to o.52 $\pm$ 0.04 over the potential range of -0.2 to -0.8 V, for all temperatures which indicates symmetry in the activation barrier.

Smaller ring currents than those predicted from the collection efficiency suggest a following reaction after the electron transfer. This could also be inferred from the shape of the oxidation curves, which show a slow rise rather than a steep rise. As the temperature is increased the following reaction is more obvious (Figure 18).

Electrochemistry of selenium is very similar to that of sulfur. Selenium solutions in DMSO also consist of Se_6, Se_7, and Se_8 rings, as shown in our HPLC studies and other works previously reported in CS_2 (41). Electrochemical reactivity for the different selenium fractions could not be determined due to their small concentrations. From the reaction of metallic cadmium and selenium solutions (Table III), it is apparent that Se_6 and Se_7 will be more reactive than Se_8. However, Se_6 and Se_7 may be adsorbed on the cadmium or the electrode surface. The reduction of selenium also presents a kinetic step in the charge transfer, as shown from plots i_D versus $w^{\frac{1}{2}}$ (Figure 8). Standard heterogeneous rate constants showed that this reaction is slower than that of sulfur. The formation of a film on the electrode surface was also observed but it does not appear to affect the kinetic process. While the composition of the film was not investigated, it is reasonable to assume the formation of a Au-Se surface compound.

Solubility of selenium in DMSO was found to be 4.3×10^{-5}F. at room temperature, and increasing with temperature as shown in Figure 5. Addition of sulfur in concentrations up to 0.25 mF. enhanced the solubility of selenium, perhaps due to the formation of Se_6S_2 or Se_4S_4 as calculated from the slopes of the curves in Figure 6. A new peak in the HPLC separation of sulfur-selenium mixtures (Figure 31) with a capacity factor equal to 2.96 indicates the formation of Se_5S_3, according to Steudel (42).

Bartlett (58, 59) proposes that S_8 is nucleophilically attacked by CN^- to form SCN^- or by triphenylphosphine to form $(C_6H_5)_3PS$. These reactions open the sulfur rings. According to this view the successive reactions of triphenylphosphine or CN^- with sulfur, and with the intermediate products, are nucleophilic displacement reactions. Once the sulfur ring is opened, the remaining chain is further attacked by CN^- or triphenylphosphine until the chain is completely consumed. In the formation of CdS or CdSe this may be the process, with the electrode surface acting as a nucleophile to open the sulfur ring.

In summary, from our results it is clear that cadmium deposition is not the limiting factor in the reaction of formation of CdS and CdSe. The reaction of S_8 with cadmium is slow and the reaction with selenium is even slower. Adsorption of S_6 and S_7 on the surface will produce deposits of CdS with excess sulfur, which are not as good material for phoelectrochemical cells.
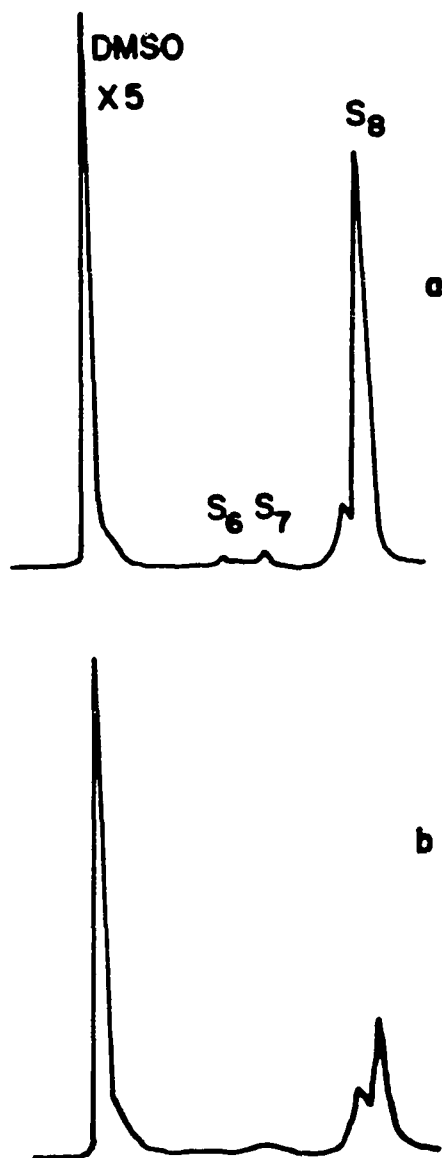
Figure 31. HPLC Separation of a Mixture of Saturated Selenium and Sulfur 1×10^{-7} F. in DMSO.

REFERENCES

1. A. Heller, Solar Energy 29, 153 (1982); and B. Miller, Electrochim. Acta, 25, 29 (1980).

2. H. Gerischer, J. Electroanal. Chem. Interfacial Electrochem., 58, 263 (1975).

3. A.B. Ellis, S. W. Kaiser, and M. S. Wrighton, J. Am. Chem. Soc., 99 2939 (1977); Ibid 98, 6855 (1977).

4. K. Rajeswar, P. Sing, and J. Dubow, Electrochim. Acta, 23, 1117 (1978).

5. T. S. Jayadeviah, Appl. Phys. Lett., 25, 399 (1974).

6. A. J. Nozik, Ann. Rev. Phys. Chem., 29. 189 (1978).

7. A. T. Fahrenbruch, J. Cryst. Growth, 39, 73 (1977)

8. M. A. Russak, J. Reichman, H. Witzke, S. K. Deb, and S. N. Chen, J. Electrochem. Soc., 127, 725 (1980).

9. J. W. Sheroham. J. Electrochem. Soc., 128, 1817 (1981).

10. K. L. Chopra, D. K. Pandya, and R. C. Kainthla, J. Electrochem Soc., 127, 277 (1980).

11. R. A. Boudreau and R. D. Rauh, J. Electrochem. Soc., 130, 513 (1983).

12. D. R. Pratt, M. E. Langmuir, R. A. Boudreau, and R. D. Rauh, J. Electrochem. Soc., 128, 1627 (1981).

13. I. Kaur, D. K. Pandya, and K. L. Chopra, J. Electrochem Soc., 127, 943 (1980).

14. G. A. Kitaer and T. S. Tarekhova, Russ. J. of Inorg. Chem., 15, 25 (1970).

15. T. H. Weng, J. Electrochem. Soc., 117, 725 (1970); Ibid, 126, 1820 (1979).

16. B. Miller, A. Heller, M. Robbings, S. Menezes, K. C. Chang and J. Thomson Jr., _J_. Electrochem. Soc., 124, 1019 (1977).

17. A. M. Redon, _J_. Electrochem. Soc., 127, 2023 (1980).

18. M. Neuman and K. Kalyanasundaram, Ber. Bunsenges. Phys. Chem., 85, 1112 (1981).

19. G. Hodes, J. Manassen, and D. Cahen, _J_. Electrochem. Soc., 127, 2252 (1980).

20. Xu-Rui Xiao, and H. Ti Tien, _J_. Electrochem. Soc., 130, 55 (1983).

21. G. Hodes, J. Manassen, and D. Cahen, Nature, 262, 403 (1976).

22. G. Hodes, J. Manassen, and D. Cahen, _J_. Electrochem. Soc., 125, 1623 (1978).

23. B. Miller and A. Heller, Nature, 262, 680 (1976).

24. B. Miller and M. S. Kazacos, _J_. Electrochem. Soc., 127, 2378 (1980) and references therein.

25. H. Gobrecht, H. D. Liess, and A. Tausend, Ber. Bunsenges. Phys. Chem., 67, 930 (1963).

26. M. P. R. Panicker, M. Knaster, and F. A. Kroger, _J_. Electrochem. Soc., 125, 566 (1978).

27. M. Tomkiewics, I. Ling, and W. S. Parsons, _J_. Electrochem. Soc., 129, 2016 (1982).

28. G. P. Power, D. R. Peggs, A. J. Parker, Electrochim. Acta, 26, 681 (1981).

29. Y. Ueno, H. Minoura, T. Nishikawa, and M. Tsuiki, _J_. Electrochem. Soc., 130, 43 (1983).

30. D. K. Roe, L. Wenzhao, and H. Ferischer, _J_. Electroanal. Chem., 136, 323 (1982).

31. A. S. Baranski and W. R. Fawcett, _J_. Electrochem. Soc., 127, 766 (1980).

32. A. S. Baranski, W. R. Fawcett, A. McDonald, R. M. DeNobriga, and J. R. McDonald, _J_. Electrochem. Soc., 128, 963 (1981).

33. A. S. Baranski, W. R. Fawcett, K. Gatner, A. C. McDonald, J. R. McDonald, and M. Selen. _J_. Electrochem, Soc., 130, 579 (1983).

34. H. Hogle, Master's Thesis, Portland State University, Portland, Oregon, 1982.

35. C. K. Mann and K. K. Barnes, "Electrochemical Reactions in Nonaqueous Solvents", Marce; Dekker, New York, 1970, chapter 14.

36. J. Badoz-Tambling, R. Bonnaterre, G. Cauquis, M. Delmar, and G. Demage, _Electrochim. Acta_, 21, 119 (1976), and references therein.

37. W. Giggenbach, _Inorg. Chem._, 11, 1201 (1972).

38. W. Giggenbach, _Inorg. Chem._, 10, 1306 (1971).

39. R. Steudel, "Topics in Current Chemistry #102, Homocyclic Sulfur Molecules", F. L. Boschke, Ed., Berlin, GDR, 1982.

40. F. N. Tebbe, E. Wasserman, W. G. Peet, A. Vatvars, and A. C. Hayman, _J. Am. Chem. Soc._, 104, 4971 (1982).

41. R. Steudel and E. M. Strauss, _Z. Naturforsch._, 36b, 1985 (1981).

42. R. Steudel and R. Laitinen, "Topics in Current Chemistry, #102, Cyclic Selenium Sulfides", F. L. Boschke, Ed., Berlin, GDR, 1982.

43. A. N. Frumkin and L. N. Nekrasov, _Dokl. Akad. Nauk. SSSR_, 126, 115 (1959).

44. A. N. Frumkin, L. N. Nekrasov, V. G. Levich, and Y. B. Ivanov, _J. Electroanal. Chem._, 1, 84 (1959).

45. V. G. Levich, _Acta Physiocochim. URSS_, 17, 257 (1942).

46. W. J. Albery and M. L. Hitchman, "Ring-Disc Electrodes". Oxford University Press, London, 1971, p 17.

47. T. Fujinaga, T. Kuwamoto, S. Okazaki, and M. Hojo, _Bull. Chem. Soc. Jpn._, 53, 2851 (1980).

48. D. T. Sawyer, R. P. Martin, W. H. Doub, and J. L. Roberts, _Inorg. Chem._, 12, 1921 (1973).

49. J. Paris and V. Plichon, _Electrochim. Acta_, 26, 1823 (1981).

50. J. W. Shultze, F. D. Koppitz, and M. M. Lohrengel, _Ber. Bunsenges. Phys, Chem._, 78, 693 (1974).

51. D. M. Kolb, M. Przasnyki, and H. Gerischer, _J. Electroanal. Chem._, 54, 25 (1974).

52. A. M. Bass, _J. Chem. Phys._, 19 1291 (1953).

53. B. Meyer, M. Gouterman, D. T. Oomen, K. Spitzer, and T. Stroyer-Hansen, "Sulfur Research Trends", R. F. Gould, Ed., New York, 1972, p 53.

54. G. J. Janz and R. P. T. Tomkins, "Nonaqueous Electrolytes Handbook", Academic Press, 1972.

55. D. L. McMasters, R. B. Dunlap, J. R. Kuempel, L. W. Kreider and T. R. Shearer, _Anal. Chem._, _39_, 103 (1967).

56. P. D. Bartlett, G. Lohaus, and C. D. Weis, _J. Am. Chem. Soc._, _83_, 103 (1961).

57. R. Steudel, "Chemistry of the Non-Metals" W. de Gruyter: New York, 1977, p. 208.

58. A. J. Bard and L. R. Faulkner, "Electrochemical Methods. Fundamentals and applications" John Wiley & Sons. New York (1980), p. 290.